# Discovery of naturally occurring *ESR1* mutations in breast cancer cell lines modelling endocrine resistance

Lesley-Ann Martin[1$*], Ricardo Ribas[1$], Nikiana Simigdala[1$], Eugene Schuster[1$], Sunil Pancholi[1], Tencho Tenev[1], Pascal Gellert[1], Laki Buluwela[2], Alison Harrod[2], Allan Thornhill[3], Joanna Nikitorowicz-Buniak[1], Amandeep Bhamra[4], Marc-Olivier Turgeon[5], George Poulogiannis[5,6], Qiong Gao[1],Vera Martins[7], Margaret Hills[7], Isaac Garcia-Murillas[1], Charlotte Fribbens[1], Neill Patani[1], Matthew Sikora[8], Nicholas Turner[1], Wilbert Zwart[9], Steffi Oesterreich[8], Jason Carroll[10], Simak Ali[2], Mitch Dowsett[1,7]

[1]Breast Cancer Now Toby Robins Research Centre, Institute of Cancer Research, London, SW7 3RP, UK; [2]University of London Imperial College, CRUK Labs, Division of Cancer, London, W12 0NN, UK; [3] Centre for Cancer Imaging, Institute of Cancer Research, Sutton, SM2 5NG, UK, [4]Proteomic unit, Institute of Cancer Research, London, SW7 3RP, UK; [5]Division of Cancer Biology, The Institute of Cancer Research, London, SW3 6JB, UK; [6]Division of Computational and Systems Medicine, Department of Surgery and Cancer, Imperial College London, SW7 2AZ, UK, [7]Ralph Lauren Centre for Breast Cancer Research, Royal Marsden Hospital, London, SW3 6JB, UK; [8]University of Pittsburg, Department of Pharmacology and Chemical biology, Pittsburg, PA 15213, USA; [9]Netherlands Cancer Institute, Department of Molecular Pathology, Amsterdam, 1066CX, Netherlands; [10]Cancer Research UK Cambridge Institute, University of Cambridge, Cambridge, CB2 0RE, UK.

[$] These authors contributed equally to this manuscript

**Running title:** *ESR1* mutations occur naturally in cell models of endocrine resistance

[*]To whom correspondence should be addressed:
Lesley-Ann Martin, Breast Cancer Now Toby Robins Research Centre, Institute of Cancer Research, London, SW7 3RP, UK, phone: +44 (0) 207 153 5329
(email: Lesley-ann.martin@icr.ac.uk)

## Abstract

Resistance to endocrine therapy remains a major clinical problem in breast cancer. Genetic studies highlight the potential role of estrogen-receptor-α (*ESR1)* mutations, which show increased prevalence in the metastatic, endocrine-resistant setting. No naturally occurring *ESR1* mutations have been reported in *in-vitro* models of BC either before or after the acquisition of endocrine resistance making functional consequences difficult to study. We report the first discovery of naturally occurring $ESR1^{Y537C}$ and $ESR1^{Y537S}$ mutations in MCF7 and SUM44 ESR1-positive cell-lines after acquisition of resistance to long-term-estrogen-deprivation (LTED) and subsequent resistance to fulvestrant (ICIR). Mutations were enriched with time, impacted on ESR1-binding to the genome and altered the ESR1-interactome. The results highlight the importance and functional consequence of these mutations and provide an important resource for studying endocrine resistance.

## Introduction

Over 70% of breast cancers (BC) are estrogen-receptor-α (ESR1) positive at diagnosis. Estrogen mediates its effects by binding to ESR1 leading to expression of genes controlling proliferation and cell survival. ESR1 has two distinct activation domains, AF-1 and AF-2. AF-1 is regulated by phosphorylation whilst AF-2 is integral to the ligand-binding domain (LBD) and associates with coactivators, controlling the ESR1 transcriptional complex (reviewed by [1]). Classically, patients with ESR1-positive BC are treated with endocrine agents such as tamoxifen, aromatase inhibitors (AIs) or fulvestrant, which impede ESR1-signalling (reviewed by [2]). Although over 50% of ESR1-positive patients show response to endocrine therapy and estrogen-deprivation therapy reduces BC mortality by 40% [3], a large proportion relapse with *de novo* or acquired resistant disease, making it one of the greatest challenges for BC research and treatment.

Multiple mechanisms of resistance have been proposed, most of which have been identified using a limited number of ESR1-positive BC cell lines. These include aberrant cross-talk between ESR1 and growth factor signalling pathways or alterations in the balance of coactivators and corepressors (reviewed by [2, 4, 5]).

It has been known for many years that some mutations in *ESR1* can lead to ligand-independent activation, but until recently, such mutations appeared to have little clinical significance [6], as their presence in primary disease is rare. However, the prevalence of *ESR1* mutations in metastatic tumours that have recurred or progressed after endocrine therapy is far higher [7, 8, 9]. We have recently reported that the detection of these mutations in ctDNA of 39.1% of metastatic patients appears to correlate with clinical resistance to AIs [10]. The majority of *ESR1* mutations are located at two amino-acids in the LBD Y537N/C/S and D538G. Functional studies using ectopic expression of these mutations led to constitutive activity of ESR1 and conferred partial resistance to established clinical doses of tamoxifen and fulvestrant [11, 12]. However, as these mutations were engineered, the role of cellular context during acquisition of resistance with time was not explored.

In this manuscript, we report for the first time, the identification of naturally occurring *ESR1* mutations in BC cell models and their enrichment during acquisition of resistance to endocrine therapy. We show that the mutated ESR1 controls a cistrome similar to the ligand-dependent wild type (wt) ESR1 and associates with an altered protein-interactome enabling ligand-independent proliferation. Furthermore, these naturally occurring *ESR1* mutants are sensitive to fulvestrant, suggesting that this and similar agents may have applicability in patients with tumours harbouring these mutations supporting our recent clinical data [13].

## Results

### Discovery of *ESR1* mutations in models of endocrine resistance

Previously, we reported the development of long-term-estrogen-deprived (LTED) derivatives from a number of ESR1-positive BC cell lines (including MCF7, HCC1428, T47D, ZR75.1 and SUM44) [14, 15]. In general, estrogen deprivation leads to an initial quiescent population accompanied by cell death and after many weeks to outgrowth of a cell population that then proliferates independently of exogenous estrogen (Supplementary Figure 1a-d). The phenotype of the LTED cell lines varies leading to a context-specific sensitivity or resistance to additional agents [14].

As *ESR1* mutations have been associated with resistance to endocrine therapy, we explored whether these mutations or those of other genes were either enriched or acquired in the *in vitro* models described. Whole-exome sequencing from wt-MCF7 and MCF7-LTED showed an $ESR1^{Y537C}$ mutation in the MCF7-LTED at an estimated variant allele frequency (VAF) of 30%, while it was undetectable in the wt-MCF7. The mutation was validated using digital droplet (dd) PCR (Fig. 1a, b).

### *ESR1* mutations occur in LTED but not tamoxifen resistant cells

As a result of this unexpected finding, we sequenced known hotspot regions for *ESR1* [16] by Ion-Torrent in wt and LTED derivatives of MCF7, SUM44, HCC1428 and ZR-75.1, together with tamoxifen-resistant (TAMR) derivatives of MCF7 and HCC1428 and fulvestrant resistant (ICIR) derivatives of wt-MCF7, MCF7-LTED and ZR75.1-LTED (Table 1 and Supplementary Figure 2). The $ESR1^{Y537C}$ mutant was detected in the MCF7-LTED-ICIR cells at a VAF of 48% that was confirmed by ddPCR (49.8%) (Supplementary Figure 3a) but was not detected in the wt-MCF7-ICIR cells.

Comparison of the two isogenic models showed that fulvestrant resistance (Supplementary Figure 3b) occurred irrespective of the mutation. Furthermore, both ICIR derivatives showed a marked reduction in ESR1 (Supplementary Figure 3c) and a concomitant drop in expression of estrogen-regulated genes (*GREB1, PDZK1, PGR* and *TFF1*) but equivalent expression of genes associated with proliferation when compared to their respective wild-type (Supplementary Figure 3d).

Strikingly, analysis by Ion-torrent also revealed an $ESR1^{Y537S}$ heterozygous mutation in SUM44-LTED (VAF 47%). *ESR1* mutations were confirmed by Sanger sequencing, RNA-sequencing, mass spectrometry and whole-exome sequencing (Supplementary Figure 4a-g). Exome sequencing did not reveal any additional mutated genes involved in AI resistance beyond the mutation in *ESR1* nor did it reveal mutations in genes known to be drivers of BC [17] that might promote growth by other mechanisms (Supplementary Data 1).

In order to determine if the $ESR1^{Y537C}$ VAF of 30% in the MCF7-LTED cells was indicative of a mixed population of cells harbouring either $ESR1^{wt}$ or $ESR1^{Y537C}$, we assessed *ESR1* copy number by fluorescent *in-situ* hybridisation (FISH) and exome sequencing. This revealed an allelic imbalance, which on average identified two or more wild-type copies of *ESR1* and one mutant copy per cell in the MCF7-LTED, indicating 100% of the cell population harboured the mutation. In contrast, the MCF7-LTED-ICIR cells were enriched for two copies of *ESR1* per cell similar to the SUM44-LTED, accounting for the VAF of 50% again indicating every cell in the given population contained a mutation (Supplementary Figure 5).

**Temporal enrichment of ESR1 mutations during estrogen deprivation**

Analysis by ddPCR over a time course showed that the $ESR1^{Y537S}$ mutation was detectable within 12 weeks following transfer of SUM44 cells to estrogen-free medium (Fig. 1c). Thereafter, the VAF increased progressively up to 50%. In order to determine if the mutation was present in the parental population or was acquired as a result of the selective pressure of estrogen-withdrawal, we screened over $6x10^6$ matched parental SUM44 copies. Interestingly, the $ESR1^{Y537S}$ mutation was present in wt-SUM44 at an apparent frequency of approximately 1:1.000.000 (Fig. 1d), implying that the $ESR1^{Y537S}$ mutation pre-exists in a very small proportion of SUM44

cells. We further screened a second batch of SUM44-LTED and their corresponding parent cell line but no mutation was identified, suggesting this is not the only adaptive mechanism. In order to control further the potential of contamination, we screened an equivalent number of ESR1-negative SKBR3 cells and no mutation was evident (Fig.1d). Finally, to address the possibility that the Y537C mutation was also resident at low frequency in MCF7 cells, we screened three independent batches, covering over 6 x$10^6$ copies, however we were unable to identify the Y537C mutation.

**ESR1$^{Y537S}$ drives ligand-independent transcription**

To determine the function of *ESR1$^{Y537S}$*, we performed ChIP-seq with antibodies for ESR1 in asynchronous wt-SUM44 in the presence of estrogen and SUM44-LTED in the absence of estrogen. Overlap of two replicate experiments called 28,647 and 23,294 ESR1 binding events in wt-SUM44 and SUM44-LTED cells, respectively. The vast majority (80%) of the ESR1$^{Y537S}$ binding sites in SUM44-LTED cells were common to ESR1$^{wt}$ binding sites in estrogen-treated wt-SUM44 (Fig. 1e). Although 4,702 differential binding sites were called in the SUM44-LTED cells, these were not unique, but represented enriched ESR1 binding i.e they also appeared in wt-SUM44 and this was similarly the case for the 10,055 differential binding sites in wt-SUM44 that occurred in the SUM44-LTED but were not enriched to the same level (Fig. 1f).

Peak strength was evaluated at a number of target genes (Supplementary Figure 6a), where augmented ESR1$^{Y537S}$ binding was evident in SUM44-LTED compared to wt-SUM44. Furthermore, ChIP-qPCR validation assessing recruitment of ESR1$^{Y537S}$ together with FOXA1, a major pioneer factor for ESR1 [18] and CBP required for an authentic ESR1 transcriptional complex [19], showed enhanced binding to the promoters of *TFF1* and *GREB1* in the SUM44-LTED compared to wt cell line (Supplementary Figure 6b).

ESR1 binding sites in both cell lines showed a similar pattern of genomic distribution (Supplementary Figure 6c). Furthermore, the vast majority of binding motifs were similar for ESR1$^{wt}$ and ESR1$^{Y537S}$ however, significant enrichment for motifs representing the transcription factors *ESR1*, *RARA*, *PAX2*, *ANDR* and *FOXA1* were evident in relation to the enriched ESR1 peaks found in SUM44-LTED, compared to wt-SUM44, which conversely showed increased *GATA3* (Fig. 1g).

To identify the transcription targets of ESR1$^{Y537S}$, we integrated ChIP-seq and RNA-seq data from the respective cell lines. Gene set enrichment analysis (GSEA) showed that increased *ESR1*$^{Y537S}$ genomic binding correlated with increased transcription, whereas loss of binding correlated with down-regulation of genes in SUM44-LTED (Fig. 1h & Supplementary Figure 6d). We next used K-means clustering to compare the ESR1 binding patterns with expression of genes in wt-SUM44, wt-SUM44 after 1-week of estrogen deprivation and the SUM44-LTED (20-weeks of estrogen-deprivation). We identified four distinct gene sets [17] (Fig. 2a-c): GS1 consisted of classical estrogen-regulated genes such as *TFF1, GREB1, PGR* and *CCND1* which decreased in expression after 1-week of deprivation but were elevated in the SUM44-LTED. GS4 contained genes such as *FOXA1* that were enriched after the first week of estrogen-deprivation and remained active in the LTED. GS2 and 3 included genes, such as *MYC* and *JUN*, which were down-regulated in the SUM44-LTED compared to wt-SUM44. Pathway analysis of the four clusters showed enrichment of ESR1-signaling, epithelial-to-mesenchymal transition (EMT), mTORC1 complex activation and cholesterol homeostasis in the SUM44-LTED.

To address this further, we assessed the metabolic capability of the wt-SUM44 and SUM44-LTED using Seahorse (Fig 2d). No significant change in glutamine dependency was evident between the two cell lines however, the SUM44-LTED showed a significantly higher glutamine capacity and fatty acid dependency compared to the wt-SUM44. The SUM44-LTED also showed a slight but significant decrease in glucose dependency.

Lastly, we assessed the migratory ability of the cell lines (Fig. 2e). The SUM44-LTED showed a 2-fold increase ($p<0.001$, Student's t-test) in migration compared to wt-SUM44.

Collectively, these findings suggest that *ESR1*$^{Y537S}$ mediates binding events that are functionally significant and lead to expression of genes controlling proliferation, survival and EMT, in a ligand-independent manner and whilst many ESR1 binding events are similar between the two lines, differences do exist and are probably the result of, or influenced by, the cellular context.

**ESR1$^{Y537S}$ interacts with known ESR1-binding proteins**

In order to elucidate the impact of the *Y537S* mutation on the ESR1-interactome and proteome, we carried out comparative RIME (rapid immunoprecipitation with tandem mass spectrometry of endogenous proteins) and dimethyl-labelling [20] between wt-SUM44 and SUM44-LTED (Fig. 3a & Supplementary Figure 7a,b). RIME demonstrated ESR1$^{Y537S}$ associated with a similar portfolio of proteins to those seen for ESR1$^{wt}$ including ESR1 itself, as well as, PGR, TLE3, HAT1 and FOXA1 [21]. However, increased association between ESR1$^{Y537S}$ GREB1 and FOXA1 was noted, which we confirmed by Co-IP (Supplementary Figure 7c). Quantitation of proteins by dimethyl-labelling showed increased abundance of TFF1 and a slight increase in ESR1 but not FOXA1 (Supplementary Figure 7d).

Immunoblot analysis of wt-SUM44 and SUM44-LTED under basal growth conditions was assessed for changes in growth factor receptors and down stream pathways associated with endocrine resistance [2] as well as alterations in pESR1$^{ser118}$, pESR1$^{ser167}$ and PGR (Fig. 3b and Supplementary Figure 8). No significant changes in pEGFR or pERBB2 were apparent between the cell lines. A slight increase in pERK1/2 was seen in SUM44-LTED but no change in pAKT$^{ser473}$. The level of pESR1$^{ser118}$ was greater in wt-SUM44 compared to the SUM44-LTED. However, a slight increase in pESR1$^{ser167}$ was noted in the LTED model (Fig. 3b). To address this further, both wt-SUM44 and SUM44-LTED were cultured in DCC medium in the absence or presence of estrogen. In this setting, ESR1 abundance and phosphorylation profiles were similar between the SUM44-LTED in the absence of estrogen and the wt-SUM44 in the presence of estrogen. Overall, these data showed the profile of the wt-SUM44 and SUM44-LTED was similar (Supplementary Figure 7e).

As FOXA1 is an important pioneer factor regulating ESR1-driven transcription [22], and FOXA1 sites were enriched in our ChIP-seq analysis of SUM44-LTED cells, we hypothesised that it played a pivotal role in transcriptional regulation of ESR1$^{Y537S}$. siRNA knockdown of FOXA1 significantly reduced proliferation of both wt-SUM44 (42%, $p<0.001$, Student's t-test) and SUM44-LTED cells although this was more pronounced in the latter (75%, $p<0.001$, Student's t-test) (Fig. 3c). siFOXA1 also correlated with a significant reduction in expression of *TFF1* and *CCND1* (Fig. 3d),

suggesting FOXA1 plays a crucial role in the ligand-independent transcriptional activity of ESR1$^{Y537S}$.

**CRISPR analysis shows *ESR1$^{Y537S}$* controls ligand independence**

As kinase signalling has been strongly implicated in endocrine resistance resulting in ligand-independent activity of ESR1 [2], we sought an approach that would reduce the effect of this confounding influence. In this setting, wt-MCF7, which harbour *ESR1$^{wt}$*, were engineered to introduce the *ESR1$^{Y537S}$* mutation using CRISPR-Cas9 genome editing. MCF7$^{Y537S}$ cells carry one endogenous *ESR1* gene in which, *ESR1$^{wt}$* has been mutated to code for the *ESR1$^{Y537S}$* mutation, as well as *ESR1$^{wt}$*. Detailed functional analyses of MCF7$^{Y537S}$ cells are described elsewhere [23]. Proliferation assays in the absence of exogenous estrogen showed the MCF7$^{Y537S}$ was ligand-independent (Fig. 4a). Furthermore, levels of ESR1 expression between the wt and the mutated cell line were similar (Fig. 4b and Supplementary Figure 8). Analysis of ESR1 ChIP-seq from wt-MCF7 and MCF7$^{Y537S}$ in the absence of exogenous estrogen showed 3602 common peaks across the genome and 8094 unique binding events in MCF7$^{Y537S}$ (Fig. 4c, d). Furthermore, peak affinity was greater for ESR1$^{Y537S}$ across the genome whilst binding events were similarly distributed for both ESR1$^{wt}$ and ESR1$^{Y537S}$ (Fig. 4e, f). Overlay of the binding events from ChIP-seq analysis with corresponding RNA-seq from MCF7$^{Y537S}$ showed increased expression of proliferation-associated genes and known estrogen-regulated genes, which was confirmed by protein expression (Fig. 4b, g and Supplementary Figure 8). This data suggests the mutation alone is sufficient to hold ESR1 in a conformation suitable for recruitment of coactivators together with the basal transcription machinery and that these mutations may not require altered kinase profiles to be active. Of note, treatment of both cell lines with estrogen revealed 74% concordance in ESR1 binding events suggesting ESR1$^{Y537S}$ remained responsive to ligand (Fig. 4h).

Intersect of the ESR1 binding events in SUM44-LTED$^{Y537S}$ and MCF7$^{Y537S}$ (Fig. 4h) showed over 50% of the peaks called in MCF7$^{Y537S}$ were common to those in SUM44-LTED$^{Y537S}$. Overlay of the common binding events with RNA-seq showed enrichment of genes associated with Hallmark pathways such as early (p-value= $10^{-72}$, hypergeometric test) and late (p-value= $10^{-43}$, hypergeometric test) estrogen responsiveness, EMT transition (p-value=$10^{-18}$, hypergeometric test), mTORC1

signalling (p-value=$10^{-12}$, hypergeometric test) and Fatty acid metabolism (p-value= $10^{-9}$, hypergeometric test) (Supplementary Data 2). Nonetheless, differences between the cell lines highlight the influence of phenotypic nuances on the ESR1 function.

**ESR1$^{wt}$ and ESR1$^{Y537C}$ have altered genome-wide binding patterns**

Two MCF7-LTED derivatives were sequenced, of which one harboured an *ESR1$^{Y537C}$* (MCF7-LTED$^{Y537C}$) and the other *ESR1$^{wt}$* (MCF7-LTED$^{wt}$) (as confirmed by ddPCR Supplementary Figure 9a), suggesting LTED itself may not always select for mutations. Indeed, there are no previous reports of *ESR1* mutations in LTED cells. Further interrogation of the whole exome sequencing data from both MCF7-LTED models, showed an increased mutational load in the MCF7-LTED$^{Y537C}$ compared to the MCF7-LTED$^{wt.}$ However, no high impact mutations previously associated with AI-resistance [2] were evident in either cell line other than ESR1$^{Y537C}$ (Supplementary Data 1). Immunoblotting showed that while key signaling pathways appeared similar between the LTED derivatives, expression of PGR differed significantly (Supplementary Figure 9b). We therefore hypothesized that the mutant *ESR1$^{Y537C}$* and *ESR1$^{wt}$* controlled different ESR1-cistromes. To address this, genome-wide binding of ESR1 was assessed in both MCF7-LTED derivatives and the corresponding wt-MCF7. Assessment of the distribution of ESR1 binding showed increased occupancy at the promoter (<1kb) in MCF7-LTED$^{wt}$ (9.2%, p=$10^{-94}$ Chi squared test) and MCF7-LTED$^{Y537C}$ (28.4%, p=0 Chi squared test) compared to wt-MCF7 (3.3%). The converse was observed for the distal intergenic regions (Fig. 5a). To address this further, we used DiffBind and identified 4,744 differential binding events between the MCF7-LTED$^{wt}$ and wt-MCF7, 13,824 between MCF7-LTED$^{Y537C}$ and wt-MCF7 and 11,018 between MCF7-LTED$^{wt}$ and MCF7-LTED$^{Y537C}$ (FDR<5%) (Supplementary Figure 9c,d). This suggested that the ESR1$^{Y537C}$ and ESR1$^{wt}$ in the MCF7-LTED cell lines control altered cistromes in comparison to wt-MCF7, but also differed between each other. Of interest, both LTED cell lines showed increased expression of *GATA3, CDK1, RET* and *ESR1* compared to the parental cell line (Fig. 5b). However, MCF7-LTED$^{Y537C}$ showed increased expression of estrogen-regulated genes such as *PGR* and *TFF1* together with *AREG*, whilst MCF7-LTED$^{wt}$ showed increased expression of *BCL2* and *XBP1* (Fig. 5b). K-means clustering of the ChIP-seq and RNA-seq data confirmed that the ESR1$^{Y537C}$ mutation appeared to function "classically" in the absence of ligand compared to MCF7-LTED$^{wt}$. Noteworthy, both LTED derivatives

enriched for pathways associated with PI3K/AKT/mTORC compared to wt-MCF7 but differed in the downstream impact of these pathways when comparing clusters 1 and 3 (Fig. 5c-e).

We next assessed the metabolic capability of the cell lines, which was similar for both capacity and dependency on glutamine, and glucose (Fig. 5f). However, the MCF7-LTED$^{wt}$ showed higher dependency on fatty acids ($p<0.05$, one-way ANOVA and Tukey's test).

Finally, and in keeping with the SUM44-LTED, both MCF7-LTED derivatives were highly migratory compared to wt-MCF7 (Fig. 5g).

In order to further delineate the dependency of the MCF7-LTED$^{Y537C}$ on the mutant *ESR1*, we carried out a CRISPR-Cas9 reversion editing Y537C to Y537 (ESR1$^{\Delta 537C}$) (Supplementary Figure 10a,b). In keeping with our previous data, MCF7-LTED$^{Y537C}$ showed ligand-independent growth. Contrastingly, MCF7-LTED$^{\Delta 537C}$ and wt-MCF7 revealed limited proliferation in the absence of estrogen (Supplementary Figure 10c). Furthermore, MCF7-LTED$^{\Delta 537C}$ switched to estrogen dependency and phenocopied the response of wt-MCF7 to fulvestrant (Supplementary Figure 10d,e). Immunoblotting and RT-qPCR showed that MCF7-LTED$^{\Delta 537C}$ regain estrogen-dependency for expression of target genes, *PGR*, *TFF1*, *GREB1* and *CTSD* (Supplementary Figure 10f,g). Taken together, these data show that the *ESR1*$^{Y537C}$ mutation is paramount for the ligand-independent phenotype of MCF7-LTED$^{Y537C}$ cells.

**ESR1 mutations show altered responses to endocrine therapy**

One of the most clinically pressing questions relates to the sensitivity of ESR1 mutations to endocrine therapy. Cell lines were treated with escalating concentrations of 4-hydroxy-tamoxifen (4-OHT) or fulvestrant in the presence or absence of estrogen (Fig. 6a-c and Supplementary Figure 8). In the absence of estrogen, both wt-MCF7 and wt-SUM44 showed little sensitivity to fulvestrant, as expected. SUM44-LTED and both MCF7-LTED derivatives were sensitive to fulvestrant in the absence of estrogen confirming ESR1 ligand-independence, irrespective of mutation state. In the presence of estrogen, sensitivity to both 4-OHT and fulvestrant was reduced in the

low concentration range in SUM44-LTED compared to wt-SUM44. However, while ESR1$^{Y537S}$ was not inhibited by 4-OHT, it was by fulvestrant. Wt-MCF7, MCF7-LTED$^{Y537C}$ and MCF7-LTED$^{wt}$ all showed similar sensitivity to 4-OHT. However, MCF7-LTED$^{Y537C}$ in the presence or absence of estrogen, showed greater sensitivity to fulvestrant compared to MCF7-LTED$^{wt}$. The sensitivity of the MCF7-LTED$^{Y537C}$ model to the antiproliferative effect of fulvestrant was further supported *in vivo* (Fig 6d).

We subsequently assessed response to drugs inhibiting pathways associated with endocrine resistance such as mTORC (RAD001), ERK1/2 (U0126) and ERBB2/EGFR (lapatinib) [2]. SUM44 derivatives were resistant to the antiproliferative effects of lapatinib and U0126 and showed similar sensitivity to RAD001. The MCF7 derivatives revealed limited response to lapatinib. MCF7-LTED$^{Y537C}$ and wt-MCF7 showed a similar response to RAD001 but not U0126, where MCF7-LTED$^{Y537C}$ showed marked sensitivity in keeping with the increased levels of pERK1/2 in this cell line. The MCF7-LTED$^{wt}$ showed little anti-proliferative response to any of the agents tested suggesting this cell line has a high degree of kinase plasticity (Supplementary Figure 11a, b).

**Discussion**

Acquired resistance to endocrine therapy is a major clinical problem and the elucidations of pathways associated with relapse are of paramount clinical importance to facilitate improvement in treatment. While somatic mutations in *ANDR* have been strongly linked with lack of response to hormone therapy and/or agonist response to anti-androgens in prostate cancer, it is only recently that the importance of *ESR1* mutations in BC has been reported (reviewed by [7]). *In vitro* studies using ectopic expression cassettes suggest that the most commonly found mutations Y537S and D538G, confer ligand-independence and exhibit reduced sensitivity to tamoxifen and fulvestrant [11, 12].

We describe for the first time the identification of naturally occurring *ESR1* mutations in ESR1 positive BC cell lines. Importantly, we show that estrogen-depletion selects

for cells harbouring *ESR1* mutations, resulting in estrogen-independent growth and expression of the ESR1 transcriptome. We believe that normal culturing of BC cell lines in the presence of estrogen obviates the need for *ESR1* mutations and that only with the strong selective pressure imparted by culturing in estrogen-depleted medium are alternative growth pathways, including *ESR1* mutations enriched. Furthermore, estrogen-deprivation appears to be the primary point for enrichment, as *ESR1* mutated cells did not appear to be augmented during acquisition of resistance to tamoxifen or fulvestrant *in vitro*. This observation is analogous to our recent clinical study in which *ESR1* mutations in ctDNA of metastatic BC patients were found almost exclusively in patients that had become resistant to AI treatment [10, 13]. Additionally, treatment with fulvestrant *in vitro* appeared to enrich for the pre-existing Y537C mutation (MCF7-LTED-ICIR).

ChIP-seq, analysis suggested that $ESR1^{Y537S}$ functions in a ligand-independent manner, largely recapitulating the estrogen-bound-$ESR1^{wt}$ cistrome, which was demonstrated by the fact that ER binding sites and their genomic distribution was overwhelmingly similar in wt-SUM44 and SUM44-LTED cells. The Y537S mutation lies near helix 12 (H12), which governs the ligand-regulated actions of ESR1 via AF-2. Recent studies have suggested that Y537S enables H12 to undergo a conformational change exposing the AF2 cleft, facilitating recruitment of coregulators in the absence of hormone, leading to further stabilization of H12. In the same study, it was shown that Y537S also increased affinity for AIB1 [24]. Assessment of the $ESR1^{Y537S}$ interactome using RIME showed no increase in the association of the naturally occurring mutant ESR1 with AIB1 but did show increased association with FOXA1 and GREB1. One possible explanation for this difference is that the structural studies analysed only the ESR1 LBD and nuclear receptor interacting domain of AIB1 [24] and thus cellular context was not explored.

Despite this compelling data, indicating the mutant *ESR1* is sufficient to drive adaptation to estrogen-deprivation, the cell lines, similar to clinical samples, are heterozygote for both wt and ESR1 mutant alleles. As such, we cannot conclusively differentiate between binding events due to wt and mutant ESR1, so it is possible that the wt allele predominates in LTED. However, there is no evidence in clinical samples that all ESR1 alleles are mutated in metastatic BC cases [11 12 25 26 27 28].

Moreover, MCF7$^{Y537S}$ cells, generated by CRISPR-Cas9 mediated knockin mutagenesis, which are heterozygote for ESR1$^{Y537S}$ and express both wt and Y537S mutant ESR1, show estrogen-independent recruitment of ESR1 and coactivators to ESR1 binding regions [23]. These cells demonstrate estrogen-independent expression of ESR1 target genes and grow in an estrogen-independent manner, validating the contribution of the Y537S mutation to estrogen independence when co-expressed with ESR1$^{wt}$.

A second caveat is the role of altered kinase signaling pathways that may arise from extended growth in estrogen-depleted culture conditions to generate LTED and post-translational changes that may impact on the resistance phenotype. Our own studies and those of others have shown that altered kinase signaling can lead to ligand-independent activation of ESR1 (reviewed by [2]). Furthermore, ectopic expression of AKT has been shown to alter the genome-wide binding pattern of ESR1 [29] and that EGF induces a transcriptional program distinct from estrogen [30]. However, genomic profiling of SUM44-LTED cells harboring ESR1$^{Y537S}$ did not provide evidence for altered ESR1 binding patterns compared to wt-SUM44. Secondly, the CRISPR-Cas9 derived MCF7$^{Y537S}$ cells showed estrogen-independence in the absence of prolonged culturing in estrogen-depleted conditions. Finally, CRISPR-Cas9 editing of the Y537C allele re-established estrogen-dependence in MCF7-LTED$^{\Delta 537C}$ cells, demonstrating a requirement for the Y537C mutation for the estrogen-independence. Taken together, our results support the notion that activating mutations in the *ESR1* are sufficient for driving acquired resistance that does not necessitate changes in other signalling pathways.

Moreover, our *in vitro* data indicate that ESR1$^{Y537S/C}$ mutations are responsive to fulvestrant, as ESR1 protein expression was downregulated (Fig. 6c), although suppression of growth was less pronounced at low concentrations of the drug, indicating partial resistance of ESR1$^{Y537S}$ but not ESR1$^{Y537C}$. Nonetheless, at the predicted clinically achievable concentrations of fulvestrant[31, 32], ESR1$^{Y537S}$ was as equally sensitive as the ESR1$^{wt}$. This is in keeping with our previous clinical data, which suggests patients harbouring an *ESR1* mutation show longer progression free survival when treated with fulvestrant versus exemestane [13]. However, in contrast to Y537C, Y537S showed reduced sensitivity to 4-OHT. One explanation for these

observations is that, 4-OHT causes Y537S to stabilise H12 by the formation of a hydrogen-bond between 537S and E380, effectively reducing the potency of the drug. In contrast, binding of fulvestrant disorders H12. As such, some of the new SERM/SERD agents with enhanced pharmacokinetics capable of increasing the dynamics of H12 may show increased potency against this mutation [24].

Interestingly, MCF7-LTED$^{wt}$ show evidence of reduced ESR1 activity, with lower expression of estrogen-regulated genes such as *PGR* and increased expression of genes associated with anti-apoptotic activity [33]. Unexpectedly, LTED cells expressing ESR1$^{wt}$ were also less sensitive to fulvestrant compared to ESR1$^{Y537C}$. One explanation is that these cells already have elevated kinase activities and are thus less dependent on ESR1, highlighting once again the complexity of cellular context as well as mutation status on response to endocrine therapy.

Recent genetic studies that have identified *ESR1* mutations in metastatic, endocrine resistant BC indicate that these mutations result from the selective pressure imposed by inhibition of ESR1 activity by hormonal therapies. The results presented here provide support for this hypothesis. The independent BC cell line models identified here also provide an important resource for studying the relative contribution of *ESR1* mutations and alterations in other signalling pathways, that lead to endocrine resistance. Indeed, the genomic studies described herein provide support for the importance of kinase signalling cascades that have already been implicated in endocrine resistance by our studies, as well as those of other investigators. Our findings demonstrate that *ESR1* mutations provide an important, albeit not the only driver of acquired endocrine resistance, concordant with the clinical observation that approximately 20% of metastatic tumours harbour mutant *ESR1*. Using resistance models featuring *ESR1* mutations and those that do not involve *ESR1* mutations should prove to be valuable in aiding patient management, and for assessing new treatment approaches for endocrine resistant BC. We and others will need to consider the presence and any phenotypic effects of these and possibly other acquired/selected mutations when using these derived cell lines for mechanistic or pharmacological studies and interpreting data from them.

## Material and Methods

### Reagents

Following antibodies were used for immunoblotting: pESR1$^{ser167}$ (CST cat-5587, 1:1000), pESR1$^{ser118}$ (CST cat-2511, 1:1000), total-ESR1 (Santa-Cruz sc8002, 1:800 or Novacastra (NCL-ER-6F11), 1:1000), total-FOXA1 (Abcam Ab23738, 1:1000) total-PGR (Novocastra NCL-L-PGR, 1:500 or Santa Cruz sc-538, 1:200), pERBB2 (CST-2243, 1:1000), total-ERBB2 (CST-4290, 1:1000), pEGFR (CST-3777, 1:1000), total-EGFR (CST-2232, 1:1000), pAKT$^{ser437}$ (CST-9271, 1:1000), total-AKT (CST-9272, 1:1000), pERK1/2 (Sigma-Aldrich, 1:2000), total-ERK1/2 (CST-9102, 1:1000), TFF1 (Santa-Cruz sc28925, 1:200), RARA (Abcam Ab39971, 1:1000), cathepsin D (CTSD) (Abcam Ab6313, 1:2000), actin (Abcam Ab6276, 1:10000) and tubulin (Sigma T-9026, 1:2000). Secondary antibodies (horseradish peroxidase-linked, 1:2000) were obtained from Dako. For ChIP, the following antibodies were used: ESR1 (Santa-Cruz sc543), CBP (Santa-Cruz sc369) and FOXA1 (Abcam Ab23738). 17-β-estradiol (E) and 4-hydroxytamoxifen (4-OHT) were purchased from Sigma-Aldrich and fulvestrant (ICI182780) from Tocris Bioscience.

### Cell culture

Wt-MCF7, wt-HCC1428, wt-ZR75.1 and wt-SUM44 were purchased from the ATCC and Asterand. Cell lines were banked in multiple aliquots upon receipt to reduce risk of phenotypic drift and identity confirmed by short tandem repeats (STR) profiling. All cell lines were routinely screened for mycoplasma contamination. Wt cell lines were cultured in phenol red free RPMI supplemented with 10% foetal bovine serum (FBS) and exogenous estradiol (1nM). The respective LTED derivatives were cultured, as previously described [14, 15] in phenol red free RPMI supplemented with 10% dextran charcoal stripped FBS (DCC medium). ICI-R and TAMR cell lines were cultured in their respective basal medium supplemented with 100nM fulvestrant (ICI182780) or 100nM 4-OHT. All experiments were performed under basal conditions unless otherwise stated.

### Proliferation assays

Proliferation assays were performed as previously described for experiments involving drugs and siRNA studies [14, 15]. In summary, cells were deprived of estrogen

for 48-72 hours prior to treatment with On-target plus® siRNA for human-si*FOXA1* or non-targeting pool (si*control*) (Thermoscientific, Dharmacon). Knockdown efficacy was determined by qRT-PCR. For drug studies, cells were treated for 6 days with a medium change at day 3, as previously described [14]. To analyse growth over time, cells were cultured as detailed above in DCC-medium with or without estradiol and data recorded using an IncuCyte ZOOM live cell analyser (Essen Biomedics). Three images per well were taken every 12 hours over a 6-day period.

**qRT-PCR**

RNA was extracted using the RNeasy kit (Qiagen), quantified and reverse-transcribed with SuperScriptIII First Strand Synthesis System (Invitrogen). Taqman gene expression assays (Applied Biosystems) were used to quantify *TFF1* (Hs00907239_m1 and Hs00170216_m1), *PGR* (Hs00172183_m1), *GREB1* (Hs00536409_m1), *CTSD* (Hs00157201_m1), *ESR1* (Hs00174860_m1), *CCND1* (Hs00765553_m1) and the house-keeping genes *FKBP15* (Hs00391480_m1) and *GAPDH* (Hs99999905_m1). The relative quantity was determined using ΔΔCt, according to the manufacturer's instructions (Applied Biosystems).

**Exome sequencing**

Exome libraries were generated with SureSelect Human All Exon V5 kit and sequenced (paired-end 100bp) on an Illumina HiSeq 2500. Reads were aligned to GRCh37-lite-build37 using BWA mem (v0.7.12-r1039) [34], sorted with samtools (v1.2) [35] and further processed using picard tools (http://picard.sourceforge.net) (v1.128) with default parameters. SNVs were detected using VarScan v2.3.5 [36] with default parameters (except --mpileup 1, --output-vcf) and wild-type cell samples as baseline. Multi-mapped reads were excluded and Base Alignment Quality (BAQ) was turned off for pileup with samtools. To get high confidence somatic mutations, SNVs were filtered by using: i) processSomatic of VarScan with empirically-derived criteria: minimum VAF in LTED cells: 0.10, maximum VAF in wild-type: 0.05, P-value = 0.07; ii) fpfilter.pl from VarScan together with bam-readcount (--min-base-quality 15, --min-mapping-quality 1) to reduce number of false positives. Variants were annotated using SnpEff v4.1 B (http://snpeff.sourceforge.net/SnpEff_manual.html). Mutations were annotated with

554 Tier levels [37] using BedTools v2.22.1 [38]. ascatNGS
555 (https://github.com/cancerit/ascatNgs) was used to generate LogR and BAF values.
556 Data has been deposited in the sequence read archive: BioProject ID PRJNA390496.
557
558 **Ion Torrent**
559 DNA was amplified using Ion AmpliSeq™ Library Kit 2.0 (Life Technologies),
560 digested, Ion Xpress™ Barcode adapters ligated and purified with Agencourt AMPure
561 XP magnetic beads (Beckman Coulter). Libraries were quantified by qPCR using an
562 Ion Library Quantification Kit (Life Technologies), templated on the Ion OneTouch2
563 System (Life Technologies) and sequenced on the Ion PGM System (Life
564 Technologies). Reads were aligned by the PGM server with standard settings to the
565 reference genome hg19, samtools v1.2 was used to calculate the on-target coverage.
566 IonReporter™ (v4.4) was used for mutation calling (parameters: Data Quality
567 Stringency= 12, Downsample To Coverage= 4000, SNP/InDel/MNP Min Cov Each
568 Strand= 50, SNP/InDel/MNP Min Variant Score= 15, SNP/InDel/MNP Min
569 Coverage= 250, Hotspot Min Variant Score= 6, Hotspot Min Coverage= 150). All
570 mutations called were manually reviewed in IGV and included in the analysis if they
571 had a VAF ≥1%.
572
573 **ddPCR**
574 ddPCR assays for the *ESR1* mutations Y537S and Y537C using Taqman probes was
575 used as previously described [10]. Very low frequency mutations were only considered
576 to be present if two or more FAM-positive droplets were detected in the total of the
577 wt sample.
578
579 **Cycle sequencing for validation**
580 *ESR1* mutations were validated by cycle sequencing by eurofins genomics (Eurofins).
581 DNA was amplified using forward primer 5'- AAGTGGCTGCAGGGAGAGT-3'
582 and reverse primer 5'- TGGTGCATGATGAGGGTAAA-3'.
583
584 **Fluorescence *in situ* hybridisation (FISH)**

FISH probes hybridising at 6q25 (ESR1) and chromosome-6 (CEN6) were purchased from Empire Genomics. Cell pellets were fixed in 4% paraformaldehyde and paraffin-embedded. Five-micron sections were subjected to the SwiftFISH rapid hybridization protocol (Empire Genomics), according to the manufacture's instructions. Sections were mounted in DAPI-containing Vectashield (Vector). FISH probes signals were analysed using fluorescent microscope (Leica).

**RNA-seq**

Libraries were created after Ribo-zero rRNA removal kit (Illumina) using NEBNext Ultra Directional RNA (NEB) or Truseq Stranded Total RNA (Illumina) Library Prep Kit and sequenced using the HiSeq2500 (paired end 100bp v4 chemistry). Tophat (v2.1) and Cuffdiff (v2.2.1) [39] using default parameters (GSE100075). Kmeans clustering was performed using the kmeans function in the stats package in R. The number of clusters used was determined by the number of clusters generated in unsupervised clustering using hclust (method = complete) function in R with of a matrix of correlation-based distances using the spearman method.

**ChIP-seq**

ChIP-qPCR and ChIP-seq were performed, as previously described [14, 40]. Paired-end 50 bp ChIP-seq data were generated by rapid-mode HiSeq. Reads were aligned to the Human Reference Genome (assembly hg19) using BWA [34] removing all reads with a quality score <15. Peaks were called using MACS2 (v2.1.0.20150420) [41] with default parameters. Only binding events that occurred in two biological replicates were considered differential binding sites using Diffbind v1.14.5 [42] and R v3.2.1. Motif analysis was performed using centrimo (500bp centered on summit of peak) (http://meme-suite.org/) (GSE100074). Bar charts were generated with ChIPseeker package in R [43].

**GSEA**

Integration of RNA-seq and ChIP-seq diffBind data were carried out using GSEA, as previously described [44]. In summary, all genes assessed using RNA-seq were ranked and weighted by their mean Log2 fold change. Lists of genes that overlapped with

regions showing significant differential binding were identified. These data were then analysed using the GSEA v2.0.13 GSEA Pre-ranked tool. The default setting was applied. Finally, additional analysis of gene sets (e.g. overlaps between significant binding events and closest genes that are significantly differentially expressed) were performed using the Molecular Signature Database (http://software.broadinstitute.org/gsea/msigdb/annotate.jsp) to compute overlaps with Hallmark gene sets that represent well-defined biological states or processes. Significance of overlap between gene sets was determined by hypergeometric test.

**RIME and dimethyl-labelling**

RIME [21] and stable isotope dimethyl-labelling [20] were performed, as previously described. The wt-SUM44 and SUM44-LTED were labelled with the medium and light isotope reagent, respectively. Labelled samples were pooled at an approximate 1:1 ratio, dried down and fractionated using 12cm IPG strip pH 3-10, as previously described [45]. RIME and dimethyl-label fractions were desalted (SUM SS18V, The Nest Group Inc) and run through LC-MS/MS using LTQ Velos Orbitrap MS. The data acquisition mode was set, as previously described [45]. Raw data for RIME and dimethyl-labelling were analysed using MaxQuant 1.5.1.0 [45, 46]. Search parameters were as previously described [45]. All proteomics data are deposited within the PRIDE database (PXD004807).

**Identification of Mutation at Protein Level using ddMS2/PRM**

ESR1-RIME samples were subjected to ddMS2-PRM analysis in order to verify the presence of wt and mutated serine or cysteine in the SUM44-LTED and MCF7-LTED samples, respectively (Supplementary Data 3). The analysis was performed using a Q-Exactive HF mass spectrometer (Thermo Scientific, Hemel Hempstead, UK). For each analysis, three biological replicates with two technical replicates were run. Heavy peptides were purchased from Thermo Fischer Scientific (PEPOTEC, grade 3). Reversed phase chromatography was performed on a Dionex UltiMate 3000 RSLC nano system (Thermo Fisher Scientific, Hemel Hempstead, UK) using an Acclaim PepMap100 C18 trap cartridge (0.5 mm i.d. x 5 mm, 5 μm bead size, 100 Å pore size; loaded in a bi-directional manner). Peptides were resolved on a 75 μm I.D. 50 cm

C18 Easy-Spray packed emitter column (2 µm particle size; PepMap RSLC, Thermo Scientific, Hemel Hempstead, UK) over 90 min using a three-step gradient of 96:4 to 50:50 buffer A:B (t = 0 min 4% B, 0.5 min 4% B, 12.0 min 10% B, 43.0 min 25% B, 90.0 min 50% B) (buffer A: 2% acetonitrile/0.1% formic acid; buffer B: 80% acetonitrile/0.1% formic acid) at 250 nL per min. Peptides were ionised by electrospray ionisation using 1.8 kV applied using the Easy-Spray ion Source. Sample was infused into the mass spectrometer directly from the packed emitter (5 µm exit bore). The ion transfer tube was heated to 275°C and the S-lens set to 50%. MS/MS were acquired using parallel reaction monitoring (PRM) and data dependent (ddMS2) acquisitions based on a full FT-MS scan from 350 to 1850 m/z at 120,000 resolution, with a target Automatic Gain Control (AGC) value of 3,000,000 and a maximum injection time of 50 ms. No internal lock mass calibrant was used. 8 PRM scans were triggered (FT-Orbitrap scans at 30,000 resolution, AGC target 2e5, 100 ms maximum injection time, normalised collision energy 35) if an ion from scheduled inclusion list was present. Then, the top 5 most intense ions were fragmented by higher energy collision-induced dissociation (HCD) and dynamically excluded for 20 s (FT-Orbitrap scans at 30,000 resolution, AGC target 1e5, activation time 10 ms, 50 ms maximum injection time, normalised collision energy 28, selected first mass at 140 m/z). Precursor ions with unknown or single charge states were excluded from selection. Data analysis of raw MS/MS was carried out using Mascot V2.3 via Proteome Discoverer v1.4. Peak lists were searched against the human Uniprot FASTA database (20,305 sequences) containing the wild-type and mutant sequence. Spectra were searched for a match to fully-tryptic peptides with up to two missed cleavage sites. Search parameters were chosen as follows: Serine/threonine phosphorylation, Protein N-terminal acetylation, Peptide N-term glutamine to pyroGlu and oxidation of methionines were all considered as variable modifications, whereas Cysteine carbamidomethylation was selected as a fixed modification. Precursor ion mass tolerance was set to 15 ppm for the first search, fragment ion mass tolerance for ion analysed spectra was set to 0.02 Da. Resulting peptide and protein lists were grouped and validated using Scaffold v4 (Proteome Software Inc., Portland, OR). Protein identifications were automatically accepted if they contained at least two unique peptides assigned at 1% FDR. The raw data has been deposited in Passel (PASS01062).

682

683 **Immunoblotting**

684 Whole-cell extracts were generated from cells cultured under basal conditions or DCC
685 medium with or without the addition of estrogen for comparative studies where noted.
686 Equal amounts of protein resolved by SDS-PAGE and subjected to immunoblot
687 analysis. Antigen-antibody interactions were detected with ECL-reagent (Amersham,
688 UK) using the antibodies referred above.

689

690 **CRISPR-Cas9 mediated generation of the MCF7-LTED$^{\Delta 537C}$ cells**

691 Gene knockins for a modified *ESR1* exon 8, encoding a wild-type open reading frame
692 with silent mutations to facilitate PCR analysis, were made using CRISPR-Cas9
693 mediated homologous recombination in MCF7-LTED$^{Y537C}$ cells. ESR1 Gene
694 targeting was carried out using CRISPR 4834093 (5'-
695 GAGTGCTGAAATCCCTAGAA-3') cloned into a guide-RNA expression plasmid (a
696 gift from George Church; Addgene plasmid # 41824), as described previously [23]. The
697 target sequence for this CRISPR is located in intron 7, on the antisense strand, 73nt
698 from the start of *ESR1* Exon 8. For making the gene knockin, a previously described
699 *ESR1* exon 8 Y537S gene targeting donor construct [23] was modified by site-directed
700 mutagenesis to change codon 537 from Serine (TCT) to Tyrosine (TAT), as found in
701 the wild-type sequence. Additional mutations, to destroy the PAM for CRISPR
702 4834093, were made by changing a run of four C nucleotides, located 77nt 5' to the
703 start of *ESR1* Exon 8, to four G nucleotides. Genome editing, detection of gene
704 targeting events and sequence characterisation of gene targeted alleles were carried
705 out as described previously [23], with the exception that following transfection, cells
706 were recovered in full medium supplemented with 10% FCS, and Exon 8 knockin
707 clones identified through stochastic cloning.

708

709 **Energy Phenotype and Mito Fuel Flex Analysis**

710 SUM44 and MCF7 cells were plated at a confluency of 1.0 x $10^4$ per well in a 96-well
711 Searhorse cell culture microplates and incubated in a 5% $CO_2$ incubator at 37 °C
712 overnight. The next morning, culture media was replaced with pH-adjusted (pH = 7.4
713 ± 0.1) bicarbonate-free DMEM with 10 mM glucose, 1 mM sodium pyruvate, and 2

mM L-Glutamine. The plate was then incubated at 37 °C for 1 hr in a non-$CO_2$ incubator. For the Mito Fuel Flex test, oxygen consumption rates were measure using the Searhorse XF Mito Fuel Flex Test Kit (Agilent, 103260-100) on an XFe96 Analyzer. Cell numbers were normalized using CyQuant (ThermoFisher, C35012).

**Cell Migration Assay**

Cells growing in basal media were washed several times with phenol red free RPMI1640 containing 1% DCC-FBS. A total of 2.5 x $10^4$ cells were seeded into the upper chambers of Corning FluoroBlok 96-multiwell insert system plates (Corning, UK). The lower chambers were filled with RPMI1640 containing 1% DCC-FBS plus 100ng/ml human recombinant EGF, as chemo-attractant, and plates were incubated at 37°C. After 16 hours, the medium was removed from the lower chambers and wells were washed with PBS. PBS containing 1μM calcein AM (Invitrogen) was added to the lower chambers and the plates were incubated at 37°C for 30 min. Fluorescence intensity was measured from the bottom of the plates using a 490nm excitation filter and a 520nm emission filter in a Victor X5 plate reader (PerkinElmer). Data is expressed as the mean of 8 replicates technical replicates.

**Human tumour xenografts modelling relapse on AI therapy**

*In vivo* studies were carried out in ovariectomized 8- to 12-week-old female BALB/c-nude mice in accordance with Home Office guidelines and approved by the Institute of Cancer Research Ethics Committee. Xenografts modelling patients resistant to AI were initiated by innoculating MCF7-LTED$^{Y537C}$ ($10^7$) cells in basement membrane matrix (Matrigel; BD Biosciences) into the right flank of each animal. Once tumours reached c. 7mm in size, they were size matched and mice treated with either 5mg per kg fulvestrant once per week or vehicle control. The study operator was blinded to treatment. Tumour growth was assessed twice weekly in both arms by caliper measurements of the two largest diameters. Volumes were then calculated according to the formula: $a \times b^2 \times \pi/6$, where $a$ and $b$ are orthogonal tumour diameters. Tumour volumes were then expressed as median relative fold change in volume at the start of treatment. At the end of study, data was available for 7 animals in the control arm and

9 animals in the fulvestrant treatment arm. Overall statistical differences between the treatment and control arms were calculated using an unpaired t-test.

**Statistics analysis**

Statistical methodologies pertinent to each method is held within the sections above.

**Data Availability**

The data supporting the finding from this manuscript have been deposited as follows. Whole exome sequencing has been deposited in the sequence read archive BioProject ID PRJNA390496. RNAseq and ChIP-seq data have been deposited with the NCBI gene expression omnibus (GEO) (http://ncbi.nlm.nih.gov/geo/): ChIP-seq data for wt-MCF7, MCF7-LTED$^{wt}$, MCF7-LTED$^{Y537C}$ wt-SUM44 and SUM44-LTED (GSE100074), RNA-seq (GSE100075) for wt-MCF7, MCF7-LTED$^{wt}$, MCF7-LTED$^{Y537C}$, wt-SUM44 and SUM44-LTED. CRISPR-cas9 MCF7$^{Y537S}$ ChIP-seq and RNA-seq data (GSE78286) [23]. All proteomics datasets are deposited within the PRIDE database (PXD004807) or Passel (PASS01062) for targeted sequencing.

**Acknowledgements**

This study was supported by Breast Cancer Now. We also acknowledge NHS funding to The Royal Marsden Hospitals NIHR biomedical Research centre and the generous funding from The Arthur Foundation in support of JN-B. SA and LB are funded by CRUK (C37/A18784), AH is supported by a PhD studentship from CRUK Imperial Centre. We also would like to thank the High-Throughput Genomics Group at the Wellcome Trust Centre for Human Genetics (funded by Wellcome Trust grant reference 090532/Z/09/Z) for the generation of the Sequencing data. Finally, we would like to thank the Tumour Profiling Unit within the Institute of Cancer Research.

**Authors Contribution**

The authors contributed to this work in different capacities described as follows. Concept: LAM; Generation of resistant models: LAM, SP, NP; Experimental work:

RR, NS, SP, JN-B; droplet digital PCR: IG-M, CF, MS, SO; NT: Bioinformatics: RNA-seq, ChIP-seq, ES, RR, NS, JC, WZ; Exome sequencing: RR, QG, PG; proteomics: NS, AB; CRISPR: TT, AH, LB, SA; Fluorescent *in-situ* hybridization: VM, MH; Metabolomics: M-OT, GP; Xenograft: AT, Manuscript and display item preparation: LAM, RR, NS, SA, ES, MD. All authors reviewed the prepared manuscript.

## Competing Interests

The authors declare no competing financial interest.

## References


1. Green KA, Carroll JS. Oestrogen-receptor-mediated transcription and the influence of co-factors and chromatin state. *Nature reviews Cancer* **7**, 713-722 (2007).

2. Ma CX, Reinert T, Chmielewska I, Ellis MJ. Mechanisms of aromatase inhibitor resistance. *Nature reviews Cancer* **15**, 261-275 (2015).

3. Early Breast Cancer Trialists' Collaborative G. Aromatase inhibitors versus tamoxifen in early breast cancer: patient-level meta-analysis of the randomised trials. *Lancet*, (2015).

4. Osborne CK, *et al.* Role of the estrogen receptor coactivator AIB1 (SRC-3) and HER-2/neu in tamoxifen resistance in breast cancer. *Journal of the National Cancer Institute* **95**, 353-361 (2003).

5. Miller TW, Balko JM, Arteaga CL. Phosphatidylinositol 3-kinase and antiestrogen resistance in breast cancer. *Journal of clinical oncology : official journal of the American Society of Clinical Oncology* **29**, 4452-4461 (2011).

6. Fuqua SA, Gu G, Rechoum Y. Estrogen receptor (ER) alpha mutations in breast cancer: hidden in plain sight. *Breast cancer research and treatment* **144**, 11-19 (2014).

7. Jeselsohn R, Buchwalter G, De Angelis C, Brown M, Schiff R. ESR1 mutations-a mechanism for acquired endocrine resistance in breast cancer. *Nature reviews Clinical oncology* **12**, 573-583 (2015).

8. Hortobagyi GN, *et al.* Correlative Analysis of Genetic Alterations and Everolimus Benefit in Hormone Receptor-Positive, Human Epidermal Growth Factor Receptor 2-Negative Advanced Breast Cancer: Results From BOLERO-2. *Journal of clinical oncology : official journal of the American Society of Clinical Oncology* **34**, 419-426 (2016).

9. Wang P, *et al.* Sensitive Detection of Mono- and Polyclonal ESR1 Mutations in Primary Tumors, Metastatic Lesions, and Cell-Free DNA of Breast Cancer Patients. *Clinical cancer research : an official journal of the American Association for Cancer Research* **22**, 1130-1137 (2016).

10. Schiavon G, *et al.* Analysis of ESR1 mutation in circulating tumor DNA demonstrates evolution during therapy for metastatic breast cancer. *Science translational medicine* **7**, 313ra182 (2015).

11. Jeselsohn R, *et al.* Emergence of constitutively active estrogen receptor-alpha mutations in pretreated advanced estrogen receptor-positive breast cancer. *Clinical cancer research : an official journal of the American Association for Cancer Research* **20**, 1757-1767 (2014).

12. Toy W, *et al.* ESR1 ligand-binding domain mutations in hormone-resistant breast cancer. *Nature genetics* **45**, 1439-1445 (2013).

13. Fribbens C, *et al.* Plasma ESR1 Mutations and the Treatment of Estrogen Receptor-Positive Advanced Breast Cancer. *Journal of clinical oncology : official journal of the American Society of Clinical Oncology*, (2016).

14. Ribas R, *et al.* AKT antagonist AZD5363 influences estrogen receptor function in endocrine resistant breast cancer and synergises with fulvestrant (ICI182780) in vivo. *Molecular cancer therapeutics*, (2015).

15. Ribas R, *et al.* Identification of chemokine receptors as potential modulators of endocrine resistance in oestrogen receptor-positive breast cancers. *Breast cancer research : BCR* **16**, 447 (2014).

16. Ellis MJ, *et al.* Whole-genome analysis informs breast cancer response to aromatase inhibition. *Nature* **486**, 353-360 (2012).

17. Nik-Zainal S, *et al.* Landscape of somatic mutations in 560 breast cancer whole-genome sequences. *Nature* **534**, 47-54 (2016).

18. Carroll JS, *et al.* Chromosome-wide mapping of estrogen receptor binding reveals long-range regulation requiring the forkhead protein FoxA1. *Cell* **122**, 33-43 (2005).

19. Shang Y, Hu X, DiRenzo J, Lazar MA, Brown M. Cofactor dynamics and sufficiency in estrogen receptor-regulated transcription. *Cell* **103**, 843-852 (2000).

20. Boersema PJ, Raijmakers R, Lemeer S, Mohammed S, Heck AJ. Multiplex peptide stable isotope dimethyl labeling for quantitative proteomics. *Nature protocols* **4**, 484-494 (2009).

21. Mohammed H, *et al.* Endogenous purification reveals GREB1 as a key estrogen receptor regulatory factor. *Cell reports* **3**, 342-349 (2013).

22. Hurtado A, Holmes KA, Ross-Innes CS, Schmidt D, Carroll JS. FOXA1 is a key determinant of estrogen receptor function and endocrine response. *Nature genetics* **43**, 27-33 (2011).

23. Harrod A, *et al.* Genomic modelling of the ESR1 Y537S mutation for evaluating function and new therapeutic approaches for metastatic breast cancer. *Oncogene* **36**, 2286-2296 (2017).

24. Fanning SW, *et al.* Estrogen receptor alpha somatic mutations Y537S and D538G confer breast cancer endocrine resistance by stabilizing the activating function-2 binding conformation. *eLife* **5**, (2016).

25. Zhang QX, Borg A, Wolf DM, Oesterreich S, Fuqua SA. An estrogen receptor mutant with strong hormone-independent activity from a metastatic breast cancer. *Cancer research* **57**, 1244-1249 (1997).

26. Li S, *et al.* Endocrine-therapy-resistant ESR1 variants revealed by genomic characterization of breast-cancer-derived xenografts. *Cell reports* **4**, 1116-1130 (2013).

27. Robinson DR, *et al.* Activating ESR1 mutations in hormone-resistant metastatic breast cancer. *Nature genetics* **45**, 1446-1451 (2013).

28. Merenbakh-Lamin K, *et al.* D538G mutation in estrogen receptor-alpha: A novel mechanism for acquired endocrine resistance in breast cancer. *Cancer research* **73**, 6856-6864 (2013).

29. Bhat-Nakshatri P, *et al.* AKT alters genome-wide estrogen receptor alpha binding and impacts estrogen signaling in breast cancer. *Molecular and cellular biology* **28**, 7487-7503 (2008).

30. Lupien M, *et al.* Growth factor stimulation induces a distinct ER(alpha) cistrome underlying breast cancer endocrine resistance. *Genes & development* **24**, 2219-2227 (2010).

31. McCormack P, Sapunar F. Pharmacokinetic profile of the fulvestrant loading dose regimen in postmenopausal women with hormone receptor-positive advanced breast cancer. *Clinical breast cancer* **8**, 347-351 (2008).

32. Pritchard KI, *et al.* Results of a phase II study comparing three dosing regimens of fulvestrant in postmenopausal women with advanced breast cancer (FINDER2). *Breast cancer research and treatment* **123**, 453-461 (2010).

33. Gomez BP, *et al.* Human X-box binding protein-1 confers both estrogen independence and antiestrogen resistance in breast cancer cell lines.

*FASEB journal : official publication of the Federation of American Societies for Experimental Biology* **21**, 4013-4027 (2007).

34. Li H, Durbin R. Fast and accurate short read alignment with Burrows-Wheeler transform. *Bioinformatics* **25**, 1754-1760 (2009).

35. Li H*, et al.* The Sequence Alignment/Map format and SAMtools. *Bioinformatics* **25**, 2078-2079 (2009).

36. Koboldt DC*, et al.* VarScan: variant detection in massively parallel sequencing of individual and pooled samples. *Bioinformatics* **25**, 2283-2285 (2009).

37. Mardis ER*, et al.* Recurring mutations found by sequencing an acute myeloid leukemia genome. *The New England journal of medicine* **361**, 1058-1066 (2009).

38. Quinlan AR, Hall IM. BEDTools: a flexible suite of utilities for comparing genomic features. *Bioinformatics* **26**, 841-842 (2010).

39. Trapnell C*, et al.* Transcript assembly and quantification by RNA-Seq reveals unannotated transcripts and isoform switching during cell differentiation. *Nature biotechnology* **28**, 511-515 (2010).

40. Schmidt D, Wilson MD, Spyrou C, Brown GD, Hadfield J, Odom DT. ChIP-seq: using high-throughput sequencing to discover protein-DNA interactions. *Methods* **48**, 240-248 (2009).

41. Zhang Y*, et al.* Model-based analysis of ChIP-Seq (MACS). *Genome biology* **9**, R137 (2008).

42. Stark R, Brown GD. DiffBind: differential binding analysis of ChIP-Seq peak data. (ed^(eds) (2011).

43. Yu G, Wang LG, He QY. ChIPseeker: an R/Bioconductor package for ChIP peak annotation, comparison and visualization. *Bioinformatics* **31**, 2382-2383 (2015).

44. Mohammed H*, et al.* Progesterone receptor modulates ERalpha action in breast cancer. *Nature* **523**, 313-317 (2015).

45. Simigdala N*, et al.* Cholesterol biosynthesis pathway as a novel mechanism of resistance to estrogen deprivation in estrogen receptor-positive breast cancer. *Breast cancer research : BCR* **18**, 58 (2016).

46. Cox J, Mann M. MaxQuant enables high peptide identification rates, individualized p.p.b.-range mass accuracies and proteome-wide protein quantification. *Nature biotechnology* **26**, 1367-1372 (2008).

966

## Figure Legends

**Figure 1. Identification and characterisation of *ESR1* mutations in models of endocrine resistance (a)** Visualisation of $ESR1^{Y537C}$ identified during exome sequencing. (**b)** Digital droplet PCR (ddPCR) showing the presence of the $ESR1^{Y537C}$ mutation in MCF7-LTED. **(c)** ddPCR showing the presence of the $ESR1^{Y537S}$ mutation in SUM44-LTED. Temporal analysis showing enrichment of the mutation from wk12 post estrogen-deprivation. **(d)** ddPCR showing the presence of $ESR1^{Y537S}$ at low variant allele frequency (VAF) in wt-SUM44 but not in SKBR3. **(e)** Overlap between wt-SUM44 and SUM44-LTED ESR1 binding sites and corresponding heatmap. The heatmap depicts binding peak intensities, which are common or different between the two cell lines. The window represents ± 5kb regions from the centre of the binding event. **(f)** Comparison of the average read count between wt-SUM44 and SUM44-LTED showing peak affinity for the common and different binding events between the two cell lines. **(g)** Motif analysis of common and augmented ESR1 peaks from wt-SUM44 versus SUM44-LTED. P-value of "common peaks" based on average of 3 random selections of 2150 peaks to approximately match the number of peaks within the "augmented peak" comparisons. **(h)** GSEA was conducted comparing RNA-seq with ESR1 induced binding events in SUM44-LTED. ChIP-seq analysis was carried out using data from two biological replicates and RNA-seq from 3 biological replicates.

**Figure 2. $ESR1^{Y537S}$ controls proliferation, EMT and altered metabolism in SUM44-LTED (a)** Heatmap depicting the changes in gene expression from four identified clusters of genes that were significantly differentially expressed and bound by $ESR1^{wt}$ (wt-SUM44) or $ESR1^{Y537S}$ (SUM44-LTED). **(b)** Average log2 differences in ESR1 binding for all genes within each cluster during the course of adaptation to LTED. **(c)** Pathway analysis of the four clusters, using GSEA. Sample labels represent: +E wk0= wt-SUM44, -E wk1= 1 wk E-deprived SUM44, -E wk 20= SUM44-LTED. (**d**) Metabolic dependency and capacity of wt-SUM44 and SUM44-LTED on glutamine, fatty acid and glucose using a Seahorse XFe96 analyzer. (n=4 technical replicates). (**e**) Comparison of the migratory ability of wt-SUM44 and SUM44-LTED (n=8 technical replicates). Error bars represent mean ± SEM. Significance was assessed by Student's t-test. * $p < 0.05$, ** $p < 0.01$, *** $p < 0.001$.

**Figure 3. Identification and functional analysis of the ESR1$^{Y537S}$ interactome (a)** MS-ARC depicting ESR1 RIME data conducted on SUM44-LTED (ESR1$^{Y537S}$) versus wt-SUM44 (ESR1$^{wt}$) (n=3 biological replicates). The ranking is based on SUM44-LTED/wt-SUM44 peptide (razor and unique) counts. The length of the line represents the number of identified peptides. The longer the line, the greater the interaction with ESR1$^{Y537S}$ compared to ESR1$^{wt}$. The shorter cloud of lines shows the high degree of commonality in ESR1 binding proteins between both cell lines. **(b)** Immunoblotting showing alterations in expression of key protein markers previously associated with endocrine resistant phenotypes. **(c)** Proliferation assays following siFOXA1 in wt-SUM44 and SUM44-LTED relative to siControl in the presence and absence of E (estradiol) (n=2 biological experiments with 8 technical replicates). **(d)** Expression of estrogen-regulated genes, *TFF1* and *CCND1* following suppression of FOXA1 (n=3 technical replicates). (Error bars represent mean ± SEM, * $p<0.05$, ** $p<0.01$, *** $p<0.001$, Significance was assessed by Student's t-test).

**Figure 4. Characterisation of CRISPR-cas9 modified wt-MCF7 expressing *ESR1$^{Y537S}$* (a)** Viability assay showing MCF7$^{Y537S}$ proliferate in the absence of exogenous E compared to wt-MCF7 (n=6 technical replicates and 3 biolgical replicates). Mean growth at day12 ± SEM relative to day 0. **(b)** Immunoblotting showing alterations in the expression of ESR1, PGR, CTSD, TFF1 and RARA. **(c)** Overlap between wt-MCF7 and MCF7$^{Y537S}$ ESR1 binding sites in the absence of E and **(d)** corresponding heat map. The heatmap depicts binding peak intensities that are common or different between the wt-MCF7 and MCF7$^{Y537S}$. The window represents ± 5kb regions from the centre of the binding event. **(e)** Comparison of the average read count between wt-MCF7 and MCF7$^{Y537S}$ in the absence of E showing peak affinity in both cell lines (left) and those binding sites only significant in MCF7$^{Y537S}$ (right) (q-value <0.05). **(f)** Bar chart showing the genomic distribution of ESR1 binding sites across the genome in both cell lines. **(g)** Volcano plot showing changes in gene expression by RNA-seq as a result of differential ESR1$^{Y537S}$ binding in MCF7$^{Y537S}$ showing increased expression of estrogen-regulated and proliferation associated genes. **(h)** Venn-diagrams showing intersect between wt-MCF7 and CRISPR generated MCF7$^{Y537S}$ ChIP-seq peaks in response to ethanol (ETOH) or estradiol (E) and intersect between SUM44-LTED and MCF7$^{Y537S}$ in the absence of E.

**Figure 5. ESR1$^{wt}$ and ESR1$^{Y537C}$ regulate altered ESR1 cistrome (a)** Bar chart showing the genomic distribution of ESR1 binding sites across the genome in wt-MCF7, MCF7-LTED$^{wt}$ and MCF7-LTED$^{Y537C}$ showing altered promoter (≤1kb) and distal intergenic occupancy. **(b)** Volcano plots showing changes in gene expression by RNA-seq in MCF7-LTED$^{Y537C}$, MCF7-LTED$^{wt}$ and wt-MCF7 **(c)** Heatmap depicting the changes in gene expression of the four clusters comparing wt-MCF7 to MCF7-LTED$^{Y537C}$, wt-MCF7 to MCF7-LTED$^{wt}$ and MCF7-LTED$^{Y537C}$ to MCF7-LTED$^{wt}$. **(d)** Average log2 differences for all genes within each set for wt-MCF7, MCF7-LTED$^{wt}$ and MCF7-LTED$^{Y537C}$. **(e)** Pathway analysis of the four clusters, using GSEA. Data was derived from n=2 biological replicates for ChIP-seq and n=3 biological replicates for RNA-seq. (**f**) Metabolic dependency and capacity of wt-MCF7, MCF7-LTED$^{wt}$ and MCF7-LTED$^{Y537C}$ on glutamine, fatty acid and glucose using a Seahorse XFe96 analyzer (n=4 technical replicates). Significance was assessed by one-way ANOVA and Tukey's test. * $p < 0.05$, ** $p < 0.01$, *** $p < 0.001$ (**g**) Comparison of the migratory ability of wt-MCF7, MCF7-LTED$^{wt}$ and MCF7-LTED$^{Y537C}$ (n=8 technical replicates). Data shown is mean ± SEM. Significance was assessed by Student's t-test. * $p < 0.05$, ** $p < 0.01$, *** $p < 0.001$.

**Figure 6. Anti-proliferative effect of endocrine therapy in ESR1 mutant and wt cell lines (a)** Proliferation assays assessing response of wt-SUM44 and SUM44-LTED and **(b)** wt-MCF7, MCF7-LTED $^{wt}$ and MCF7-LTED$^{Y537C}$ to escalating concentration of fulvestrant ± E (estradiol) and 4-OHT plus E (estradiol). **(c)** Treatment of wt-SUM44, SUM44-LTED$^{Y537S}$, wt-MCF7, MCF7-LTED$^{Y537C}$ and MCF7-LTED$^{wt}$ with fulvestrant (10nM) results in loss of ESR1 expression irrespective of mutation status (n=3 biological replicates consisting of n=8 technical replicates). Data represents mean ± SEM (**d**) Xenograft models of MCF7-LTED$^{Y537C}$ in response to vehicle or fulvestrant. Data represents median fold change in tumour volume. Significance was assessed using an unpaired t-test.

**Table 1.** Identification of naturally occurring *ESR1* mutations in cell line models of endocrine sensitive and resistant breast cancer.

| Cell Line | No. Batches Screened | No. Positive Batches | Mutation | VAF (%) |
|---|---|---|---|---|
| wt-MCF7 | 4 | 0 | - | - |
| MCF7-LTED | 4 | 1 | Y537C | 30 |
| MCF7-TAMR | 1 | 0 | - | - |
| wt-MCF7-ICIR | 1 | 0 | - | - |
| MCF7-LTED-ICIR | 1 | 1 | Y537C | 50 |
| wt-HCC1428 | 1 | 0 | - | - |
| HCC1428-LTED | 1 | 0 | - | - |
| HCC1428-TAMR | 1 | 0 | - | - |
| wt-SUM44 | 2* | 1 | Y537S | 0.0001 |
| SUM44-LTED | 2* | 1 | Y537S | 50 |
| wt-ZR75.1 | 1 | 0 | - | - |
| ZR75.1-LTED | 1 | 0 | - | - |

* Second batch originated from an independent laboratory

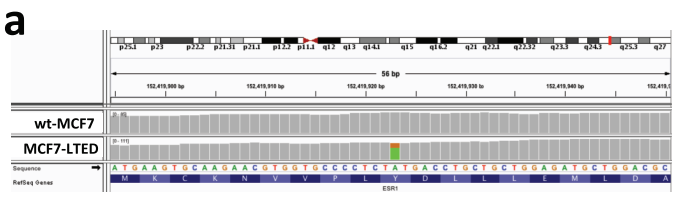


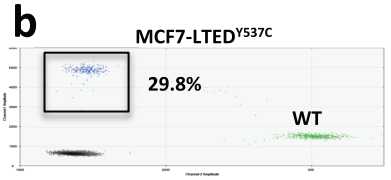


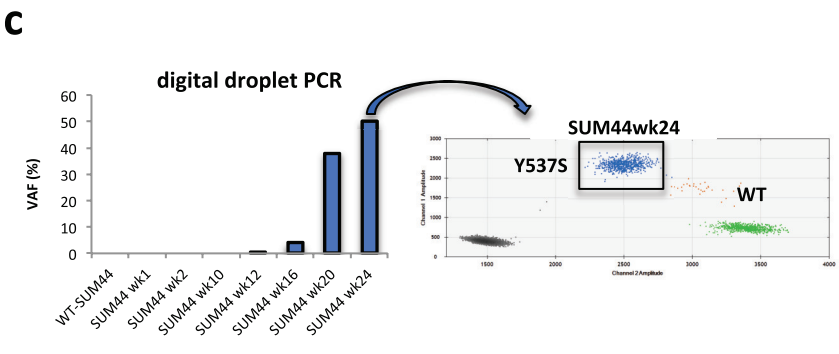


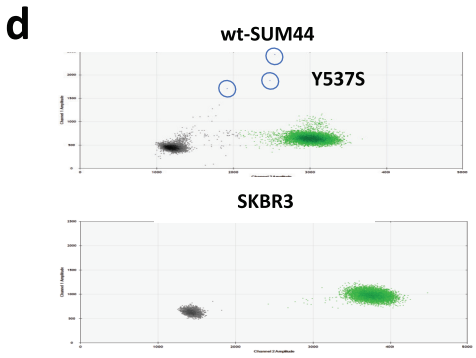


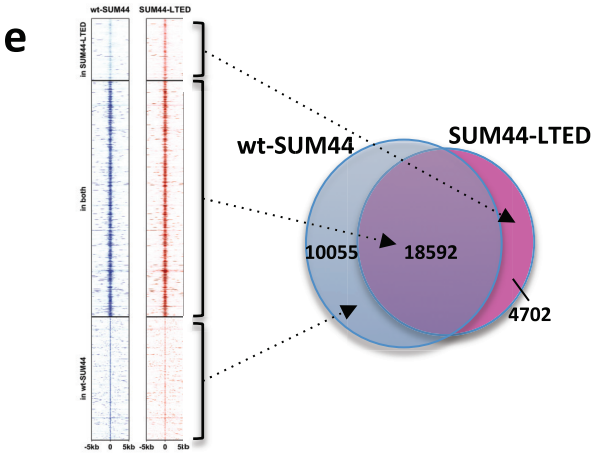


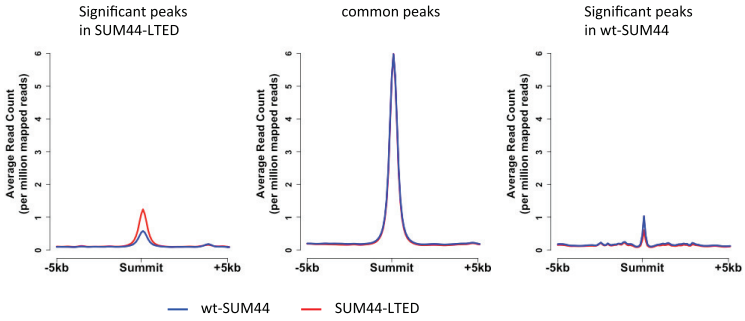


g

| Sequence Logo | Name | p-value wt-SUM44 | p-value SUM44-LTED | p-value Common |
|---|---|---|---|---|
| | ESR1 | $10^{-72}$ | $10^{-313}$ | $10^{-132}$ |
| | RARA | $10^{-48}$ | $10^{-151}$ | $10^{-73}$ |
| | FOXA1 | $10^{-21}$ | $10^{-40}$ | $10^{-33}$ |
| | PAX2 | $10^{-4}$ | $10^{-34}$ | $10^{-13}$ |
| | GATA3 | $10^{-58}$ | >0.05 | $10^{-6}$ |
| | ANDR | $10^{-5}$ | $10^{-20}$ | $10^{-4}$ |

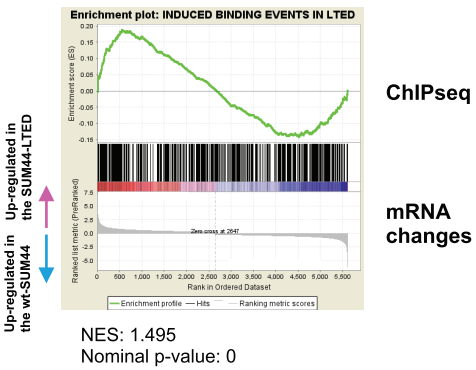

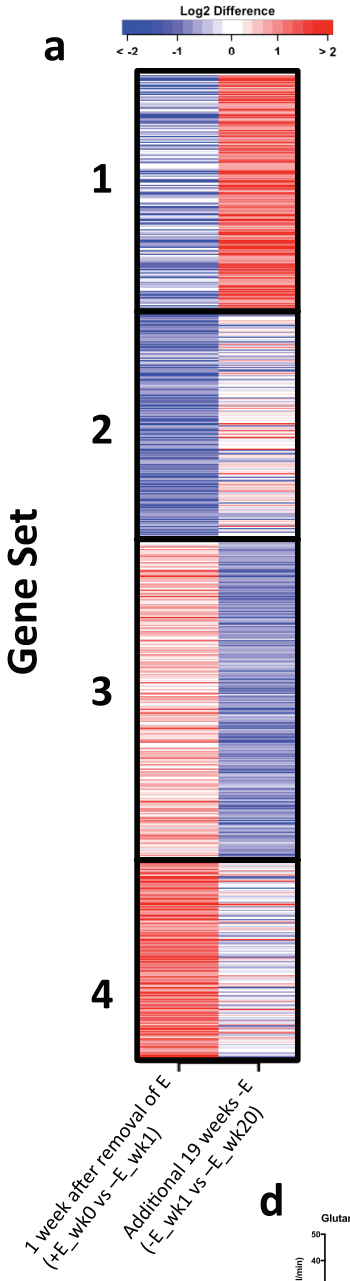


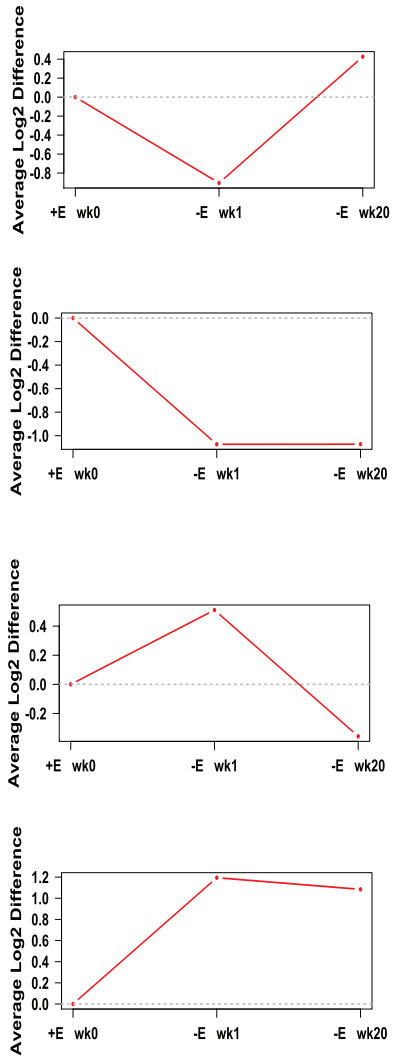


c

| Gene Set Name | FDR q-value |
|---|---|
| HALLMARK_ESTROGEN_RESPONSE_EARLY | 1.37E-42 |
| HALLMARK_ESTROGEN_RESPONSE_LATE | 1.84E-41 |
| HALLMARK_XENOBIOTIC_METABOLISM | 3.95E-09 |
| HALLMARK_P53_PATHWAY | 1.86E-07 |
| HALLMARK_EPITHELIAL_MESENCHYMAL_TRANSITION | 7.58E-07 |
| HALLMARK_HYPOXIA | 7.58E-07 |
| HALLMARK_TNFA_SIGNALING_VIA_NFKB | 7.58E-07 |
| HALLMARK_GLYCOLYSIS | 3.90E-06 |
| HALLMARK_KRAS_SIGNALING_UP | 3.90E-06 |
| HALLMARK_APOPTOSIS | 1.55E-05 |
| HALLMARK_INTERFERON_GAMMA_RESPONSE | 1.95E-05 |
| HALLMARK_MTORC1_SIGNALING | 9.29E-05 |
| HALLMARK_MYOGENESIS | 9.29E-05 |
| HALLMARK_PANCREAS_BETA_CELLS | 3.35E-04 |
| HALLMARK_FATTY_ACID_METABOLISM | 3.35E-04 |

| Gene Set Name | FDR q-value |
|---|---|
| HALLMARK_TNFA_SIGNALING_VIA_NFKB | 3.49E-23 |
| HALLMARK_ESTROGEN_RESPONSE_EARLY | 4.59E-21 |
| HALLMARK_MTORC1_SIGNALING | 6.79E-19 |
| HALLMARK_UNFOLDED_PROTEIN_RESPONSE | 1.31E-13 |
| HALLMARK_ESTROGEN_RESPONSE_LATE | 1.31E-13 |
| HALLMARK_HYPOXIA | 1.21E-11 |
| HALLMARK_P53_PATHWAY | 1.00E-10 |
| HALLMARK_UV_RESPONSE_DN | 5.60E-10 |
| HALLMARK_EPITHELIAL_MESENCHYMAL_TRANSITION | 4.36E-08 |
| HALLMARK_GLYCOLYSIS | 4.36E-08 |
| HALLMARK_IL2_STAT5_SIGNALING | 2.70E-07 |
| HALLMARK_XENOBIOTIC_METABOLISM | 2.70E-07 |
| HALLMARK_UV_RESPONSE_UP | 8.99E-07 |
| HALLMARK_INTERFERON_GAMMA_RESPONSE | 1.60E-06 |
| HALLMARK_CHOLESTEROL_HOMEOSTASIS | 5.76E-06 |

| Gene Set Name | FDR q-value |
|---|---|
| HALLMARK_MITOTIC_SPINDLE | 1.05E-24 |
| HALLMARK_G2M_CHECKPOINT | 2.69E-17 |
| HALLMARK_P53_PATHWAY | 1.15E-10 |
| HALLMARK_E2F_TARGETS | 1.23E-07 |
| HALLMARK_HYPOXIA | 1.23E-07 |
| HALLMARK_IL2_STAT5_SIGNALING | 1.23E-07 |
| HALLMARK_TNFA_SIGNALING_VIA_NFKB | 1.23E-07 |
| HALLMARK_ADIPOGENESIS | 1.99E-05 |
| HALLMARK_APICAL_JUNCTION | 7.86E-05 |
| HALLMARK_HEME_METABOLISM | 7.86E-05 |
| HALLMARK_ANDROGEN_RESPONSE | 1.25E-04 |
| HALLMARK_APOPTOSIS | 1.85E-04 |
| HALLMARK_GLYCOLYSIS | 2.76E-04 |
| HALLMARK_KRAS_SIGNALING_UP | 1.08E-03 |
| HALLMARK_UV_RESPONSE_DN | 1.39E-03 |

| Gene Set Name | FDR q-value |
|---|---|
| HALLMARK_MTORC1_SIGNALING | 2.75E-07 |
| HALLMARK_XENOBIOTIC_METABOLISM | 2.75E-07 |
| HALLMARK_E2F_TARGETS | 7.96E-06 |
| HALLMARK_HYPOXIA | 7.96E-06 |
| HALLMARK_PEROXISOME | 7.96E-06 |
| HALLMARK_UV_RESPONSE_DN | 1.24E-05 |
| HALLMARK_G2M_CHECKPOINT | 3.14E-05 |
| HALLMARK_BILE_ACID_METABOLISM | 8.54E-05 |
| HALLMARK_INFLAMMATORY_RESPONSE | 1.23E-04 |
| HALLMARK_KRAS_SIGNALING_UP | 1.23E-04 |
| HALLMARK_MYOGENESIS | 1.23E-04 |
| HALLMARK_CHOLESTEROL_HOMEOSTASIS | 3.40E-04 |
| HALLMARK_APICAL_JUNCTION | 4.92E-04 |
| HALLMARK_EPITHELIAL_MESENCHYMAL_TRANSITION | 4.92E-04 |
| HALLMARK_KRAS_SIGNALING_DN | 4.92E-04 |

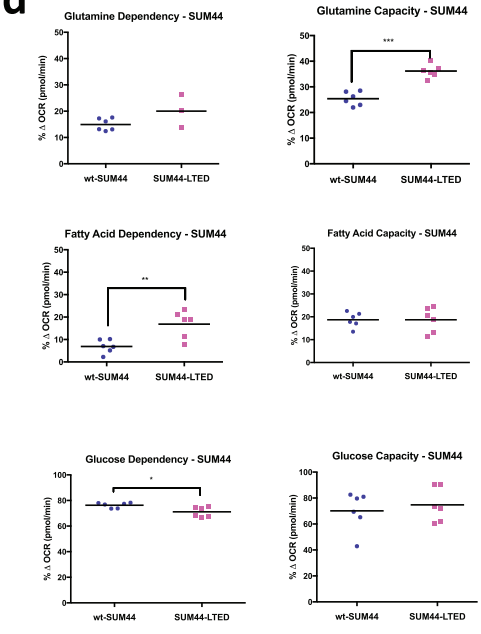


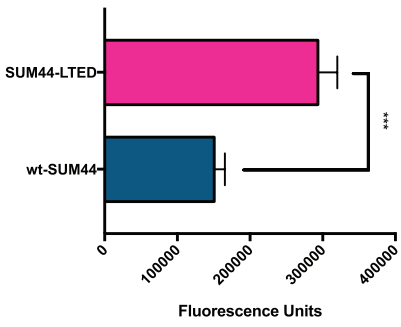

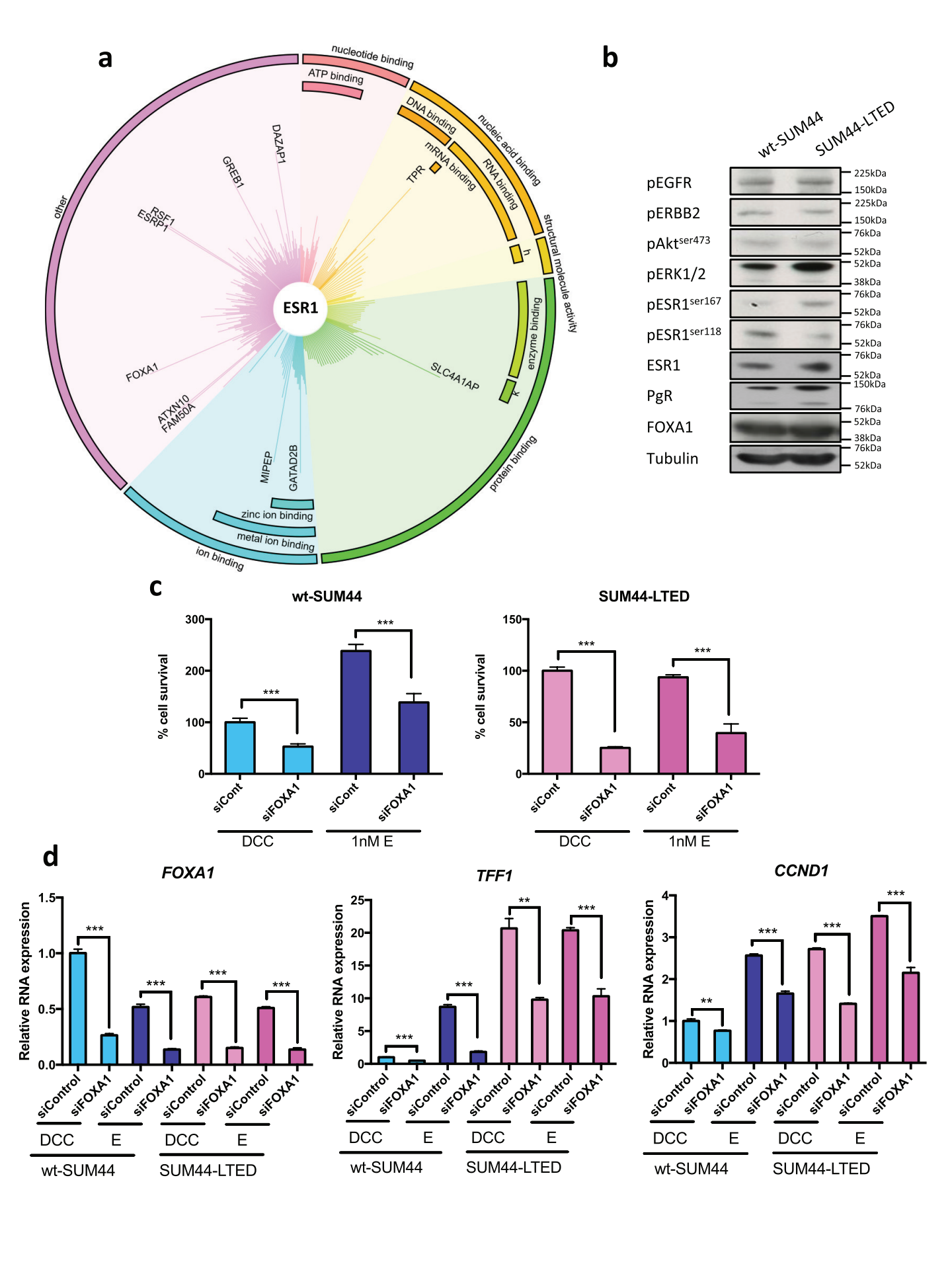
a
nucleotide binding
ATP binding
DNA binding
nucleic acid binding
mRNA binding
RNA binding
TPR
structural molecule activity
h
enzyme binding
k
SLC4A1AP
protein binding
zinc ion binding
metal ion binding
ion binding
MIPEP
GATAD2B
ATXN10
FAM50A
FOXA1
other
RSF1
ESRP1
GREB1
DAZAP1
ESR1
b
wt-SUM44
SUM44-LTED
pEGFR
pERBB2
pAkt ser473
pERK1/2
pESR1 ser167
pESR1 ser118
ESR1
PgR
FOXA1
Tubulin
225kDa
150kDa
76kDa
52kDa
38kDa
c
wt-SUM44
SUM44-LTED
% cell survival
siCont
siFOXA1
DCC
1nM E
d
FOXA1
TFF1
CCND1
Relative RNA expression
siControl
siFOXA1
DCC
E
wt-SUM44
SUM44-LTED

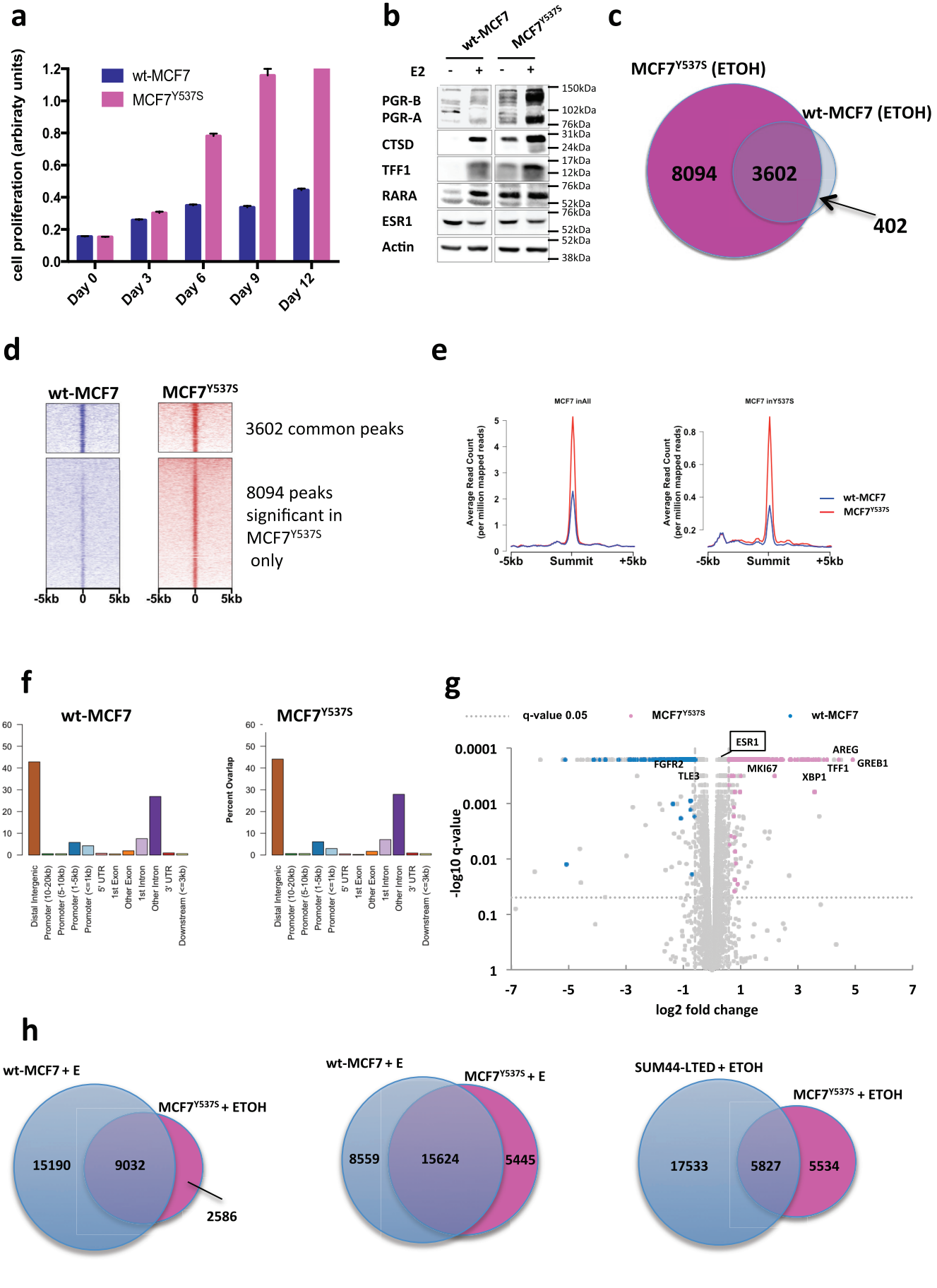
a
cell proliferation (arbiraty units)
wt-MCF7
MCF7Y537S
Day 0
Day 3
Day 6
Day 9
Day 12
b
wt-MCF7
MCF7Y537S
E2
PGR-B
PGR-A
CTSD
TFF1
RARA
ESR1
Actin
150kDa
102kDa
76kDa
31kDa
24kDa
17kDa
12kDa
76kDa
52kDa
76kDa
52kDa
52kDa
38kDa
c
MCF7Y537S (ETOH)
wt-MCF7 (ETOH)
8094
3602
402
d
wt-MCF7
MCF7Y537S
3602 common peaks
8094 peaks significant in MCF7Y537S only
-5kb
0
5kb
e
MCF7 inAll
MCF7 inY537S
Average Read Count (per million mapped reads)
wt-MCF7
MCF7Y537S
-5kb
Summit
+5kb
f
wt-MCF7
MCF7Y537S
Percent Overlap
Distal Intergenic
Promoter (10-20kb)
Promoter (5-10kb)
Promoter (1-5kb)
Promoter (<=1kb)
5' UTR
1st Exon
Other Exon
1st Intron
Other Intron
3' UTR
Downstream (<=3kb)
g
q-value 0.05
MCF7Y537S
wt-MCF7
ESR1
AREG
FGFR2
MKI67
TFF1
GREB1
TLE3
XBP1
-log10 q-value
log2 fold change
h
wt-MCF7 + E
MCF7Y537S + ETOH
15190
9032
2586
wt-MCF7 + E
MCF7Y537S + E
8559
15624
5445
SUM44-LTED + ETOH
MCF7Y537S + ETOH
17533
5827
5534

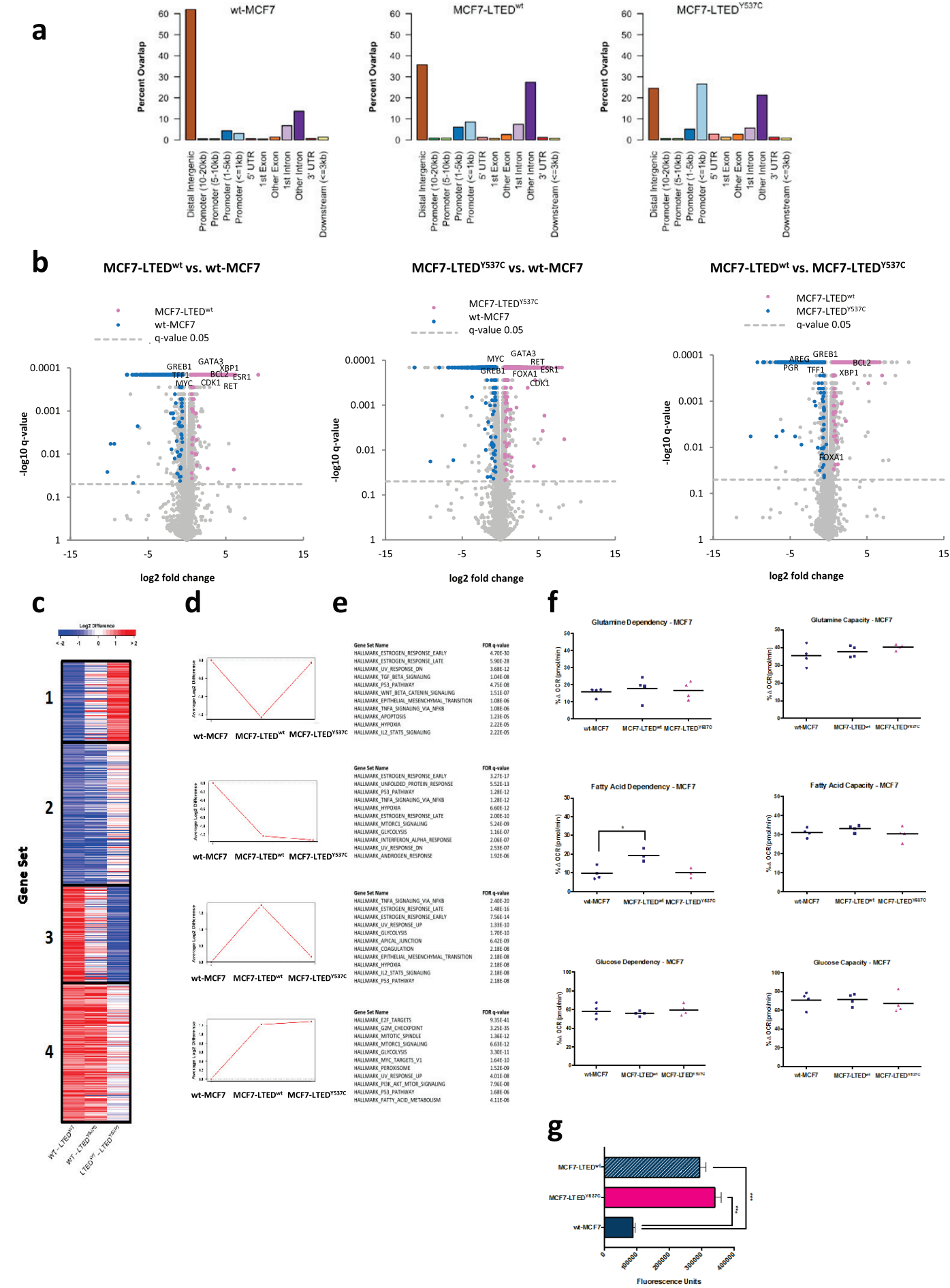
a
wt-MCF7
MCF7-LTED^wt
MCF7-LTED^Y537C
Percent Ovarlap
Distal Intergenic
Promoter (10-20kb)
Promoter (5-10kb)
Promoter (1-5kb)
Promoter (<=1kb)
5' UTR
1st Exon
Other Exon
1st Intron
Other Intron
3' UTR
Downstream (<=3kb)
b
MCF7-LTED^wt vs. wt-MCF7
MCF7-LTED^Y537C vs. wt-MCF7
MCF7-LTED^wt vs. MCF7-LTED^Y537C
MCF7-LTED^wt
wt-MCF7
MCF7-LTED^Y537C
q-value 0.05
-log10 q-value
log2 fold change
GREB1
GATA3
XBP1
TFF1
BCL2
ESR1
MYC
CDK1
RET
FOXA1
AREG
PGR
c
Log2 Difference
Gene Set
1
2
3
4
d
wt-MCF7
MCF7-LTED^wt
MCF7-LTED^Y537C
e
Gene Set Name
FDR q-value
HALLMARK_ESTROGEN_RESPONSE_EARLY 4.70E-30
HALLMARK_ESTROGEN_RESPONSE_LATE 5.90E-28
HALLMARK_UV_RESPONSE_DN 3.68E-12
HALLMARK_TGF_BETA_SIGNALING 1.04E-08
HALLMARK_P53_PATHWAY 4.75E-08
HALLMARK_WNT_BETA_CATENIN_SIGNALING 1.51E-07
HALLMARK_EPITHELIAL_MESENCHYMAL_TRANSITION 1.08E-06
HALLMARK_TNFA_SIGNALING_VIA_NFKB 1.08E-06
HALLMARK_APOPTOSIS 1.23E-05
HALLMARK_HYPOXIA 2.22E-05
HALLMARK_IL2_STAT5_SIGNALING 2.22E-05
HALLMARK_UNFOLDED_PROTEIN_RESPONSE 5.52E-13
HALLMARK_P53_PATHWAY 1.28E-12
HALLMARK_TNFA_SIGNALING_VIA_NFKB 1.28E-12
HALLMARK_HYPOXIA 6.60E-12
HALLMARK_ESTROGEN_RESPONSE_LATE 2.00E-10
HALLMARK_MTORC1_SIGNALING 5.24E-09
HALLMARK_GLYCOLYSIS 1.16E-07
HALLMARK_INTERFERON_ALPHA_RESPONSE 2.06E-07
HALLMARK_UV_RESPONSE_DN 2.53E-07
HALLMARK_ANDROGEN_RESPONSE 1.92E-06
HALLMARK_TNFA_SIGNALING_VIA_NFKB 2.40E-20
HALLMARK_ESTROGEN_RESPONSE_LATE 1.48E-16
HALLMARK_ESTROGEN_RESPONSE_EARLY 7.56E-14
HALLMARK_UV_RESPONSE_UP 1.33E-10
HALLMARK_GLYCOLYSIS 1.70E-10
HALLMARK_APICAL_JUNCTION 6.42E-09
HALLMARK_COAGULATION 2.18E-08
HALLMARK_EPITHELIAL_MESENCHYMAL_TRANSITION 2.18E-08
HALLMARK_HYPOXIA 2.18E-08
HALLMARK_IL2_STAT5_SIGNALING 2.18E-08
HALLMARK_P53_PATHWAY 2.18E-08
HALLMARK_E2F_TARGETS 9.35E-41
HALLMARK_G2M_CHECKPOINT 3.25E-35
HALLMARK_MITOTIC_SPINDLE 1.36E-12
HALLMARK_MTORC1_SIGNALING 6.63E-12
HALLMARK_GLYCOLYSIS 3.30E-11
HALLMARK_MYC_TARGETS_V1 1.64E-10
HALLMARK_PEROXISOME 1.52E-09
HALLMARK_UV_RESPONSE_UP 4.01E-08
HALLMARK_PI3K_AKT_MTOR_SIGNALING 7.96E-08
HALLMARK_P53_PATHWAY 1.68E-06
HALLMARK_FATTY_ACID_METABOLISM 4.11E-06
f
Glutamine Dependency - MCF7
Glutamine Capacity - MCF7
Fatty Acid Dependency - MCF7
Fatty Acid Capacity - MCF7
Glucose Dependency - MCF7
Glucose Capacity - MCF7
% Δ OCR (pmol/min)
g
MCF7-LTED^wt
MCF7-LTED^Y537C
wt-MCF7
Fluorescence Units

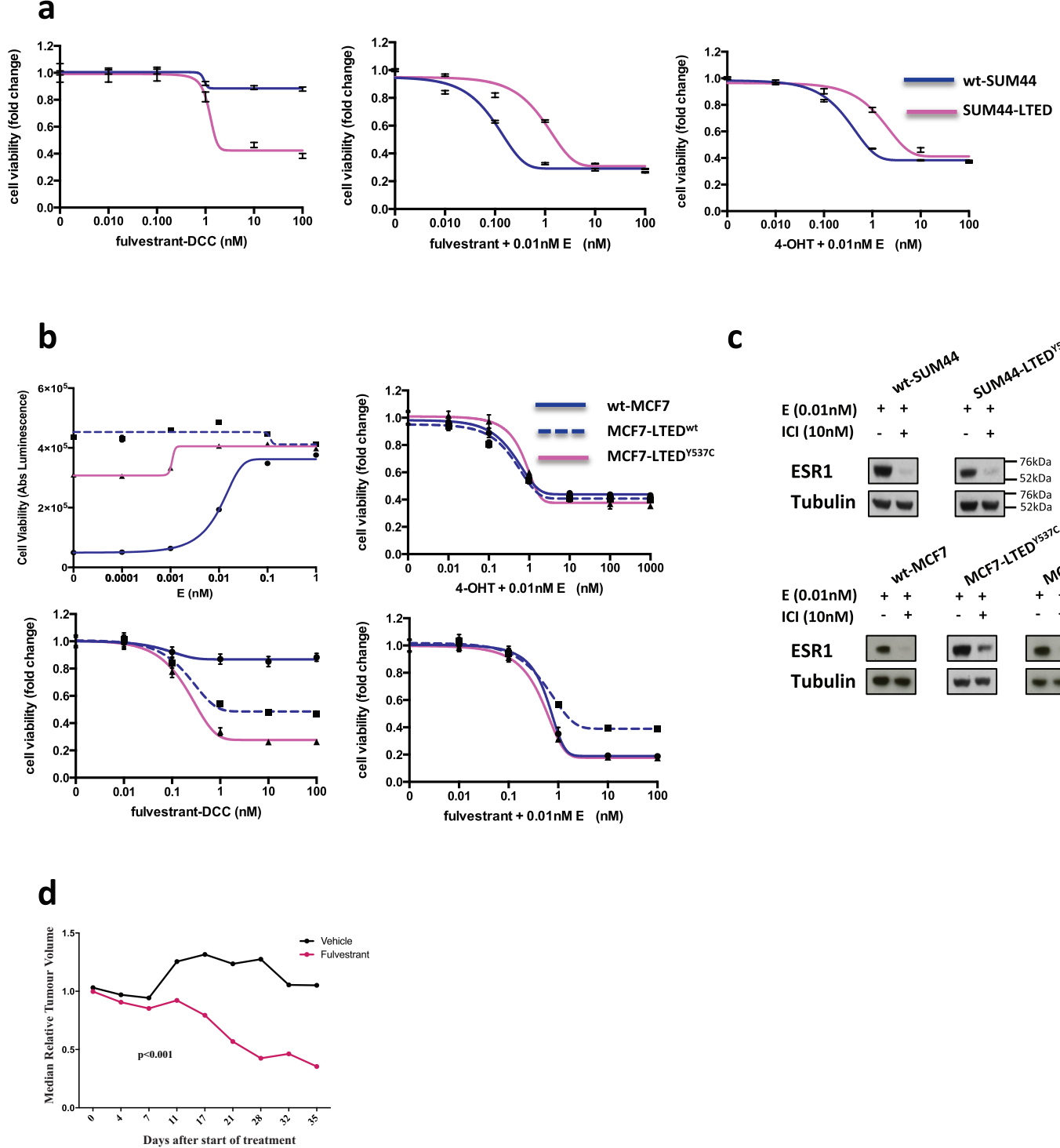
a
cell viability (fold change)
fulvestrant-DCC (nM)
fulvestrant + 0.01nM E (nM)
4-OHT + 0.01nM E (nM)
wt-SUM44
SUM44-LTED
b
Cell Viability (Abs Luminescence)
E (nM)
wt-MCF7
MCF7-LTEDwt
MCF7-LTEDY537C
4-OHT + 0.01nM E (nM)
fulvestrant-DCC (nM)
fulvestrant + 0.01nM E (nM)
c
wt-SUM44
SUM44-LTEDY537S
E (0.01nM)
ICI (10nM)
ESR1
Tubulin
76kDa
52kDa
wt-MCF7
MCF7-LTEDY537C
MCF7-LTEDwt
d
Median Relative Tumour Volume
Vehicle
Fulvestrant
p<0.001
Days after start of treatment